

Short-term variability of 10 trans-Neptunian objects

A. Thirouin^{1*}, J.L. Ortiz¹, A. Campo Bagatin^{2,3}, P. Pravec⁴, N. Morales¹,
O. Hainaut⁵, R. Duffard¹

¹*Instituto de Astrofísica de Andalucía - CSIC, Apt 3004, 18008 Granada, Spain*

²*Departamento de Física, Ingeniería de Sistemas y teoría de la Señal, Universidad de Alicante, PO Box 99, 03080 Alicante, Spain*

³*Instituto de Física Aplicada a las Ciencias y la Tecnología, Universidad de Alicante, PO Box 99, 03080 Alicante, Spain*

⁴*Astronomical Institute, Academy of Sciences of the Czech Republic, Fričova 1, CZ-25165 Ondřejov, Czech Republic.*

⁵*ESO, Karl-Schwarzschild-Str. 2, 85748 Garching bei München, Germany.*

ABSTRACT

We present our latest results about the short-term variability of trans-Neptunian objects (TNOs). We performed broad-band CCD photometric observations using several telescopes in Spain and Chile. We present results based on three years of observations and report the short-term variability of 10 TNOs. Our sample of studied targets contains classical objects: (275809) 2001 QY₂₉₇, (307251) 2002 KW₁₄, (55636) 2002 TX₃₀₀, 2004 NT₃₃, (230965) 2004 XA₁₉₂, and (202421) 2005 UQ₅₁₃, a resonant body: (84522) 2002 TC₃₀₂, a scattered target: (44594) 1999 OX₃, and two detached objects: (145480) 2005 TB₁₉₀, and (40314) 1999 KR₁₆. For each target, light curves as well as possible rotation periods and photometric amplitudes are reported. The majority of the observed objects present a low peak-to-peak amplitude, <0.15 mag. Only two objects exhibit light curve amplitudes higher than 0.15 mag: (275809) 2001 QY₂₉₇, and (307251) 2002 KW₁₄. We remark two biases in the literature, previously studied in Thirouin et al. and confirmed by this new study: a bias towards objects with a small amplitude light curve and a second one against objects with a long rotational period in the data base of published rotational periods. We derived constraints on physical properties of some targets. We also report the solar phase curves of (40314) 1999 KR₁₆, and (44594) 1999 OX₃ for solar phase angles from 0° to around 2°. Part of our discussion is focused on the study of (275809) 2001 QY₂₉₇ which turned out to be an asynchronous binary system.

Key words: Kuiper Belt: general, techniques: photometric

1 INTRODUCTION

The Edgeworth-Kuiper belt objects, usually called trans-Neptunian objects (TNOs) or Kuiper belt objects (KBOs), are known to be wellpreserved fossil remnants of our Solar system formation. Since the discovery of the first TNO (after Pluto) in 1992 by Jewitt & Luu (1993), various observational approaches to study the physical properties of TNOs have been performed, including spectroscopic, photometric and binarity studies. Our own approach to study these objects is to detect the periodic variation of their brightness as a function of time, resulting from their rotation (Thirouin et al. 2010; Ortiz et al. 2007, 2006, 2004, 2003). We analyse their rotational periods, surfaces, shapes and internal structures studying their light curves.

Less than 5 per cent of the known TNOs have well-

determined rotational periods. Moreover, Sheppard, Lacerda, & Ortiz (2008) and Thirouin et al. (2010) pointed out that the sample of studied objects is highly biased towards bright objects, large variability amplitudes and short rotational periods. Only 10 per cent of the rotational periods published are larger than 10 h. The majority of light curve amplitudes and rotational periods are published with large uncertainties or, sometimes, they are just estimations or limiting values. The sample of studied TNOs is essentially composed of bright (visual magnitude <22 mag) and large objects. We can enumerate various reasons in order to explain some of these biases. First, we must point out observational limitations. A reliable study of TNO rotational properties requires a lot of observational time on a medium to large telescope. This causes a bias towards brighter objects, but also short period and large amplitude. Another class of limitations is due to reduction problems. A reliable photometric study needs effective data reduction. Determining

* E-mail: thirouin@iaa.es

low-amplitude light curves and/or detecting long rotation periods are very time consuming and require a lot of observation time. Furthermore, 24-h aliases frequently complicate the analysis of time-series photometry.

To help debias the sample of studied objects, longer term monitoring is needed. This kind of observations is based on the coordination of observational runs with various telescopes all around the world. Using telescopes with similar characteristics in different continents allows us to observe a target continuously. In other words, if we can monitor our targets during a long time, we can detect long rotation periods and minimize the 24-h-aliases effect. In 2009 July, we carried out our first coordinated campaign between Spain and Chile. Part of this work presents results based on this coordinated campaign for TNOs. Another part of this work is dedicated to our programme on light curves of TNOs, started in 2001. In this work, we report our newest results based on observations carried out between 2008 and 2010.

This paper is divided into six sections. Section 2 will describe the observations and the data set analysed here. Section 3 will describe our reduction techniques used in order to derive periods and photometric ranges. In Section 4, we will give, for each target, a summary of our main results. In Section 5, we will discuss our results altogether. Section 6 is dedicated to the conclusion of this work.

2 OBSERVATIONS

2.1 Runs and Telescopes

We present two different approaches to study the luminosity variability of TNOs. We analysed data obtained from the coordinated campaign and data from our regular programme on light curves of KBOs.

2.1.1 Coordinated campaign

In 2009 July, we carried out our first coordinated campaign involving Europe and South America. Typically, an observational night of July in Europe starts around 22 h UT and finishes at 5 h UT, whereas an observational night in South America starts around 0 h UT and finishes at 10 h UT. Under perfect conditions and if the target is visible in both sites during the entire night, we have five extra hours of observational time. By using this approach, we have a continuous time coverage of about 15 h, thereby addressing some of the biases against long periods and the issue of the 24-h aliases. We carefully coordinated the observations, to match exactly the field of view of both telescopes, during the campaign.

In Europe, we used the Telescopio Nazionale Galileo (TNG), located at the Roque de los Muchachos Observatory (La Palma, Canary Islands, Spain). Images were obtained using the Device Optimized for the LOw REsolution instrument (DOLORES or LRS). This device has a camera and a spectrograph installed at the Nasmyth B focus of the telescope. We observed in imaging mode with the R Johnson filter and a 2×2 binning mode. The camera is equipped with a 2048×2048 CCD with a pixel size of $13.5\mu\text{m}$. The field of view is $8.6'\times 8.6'$ with a $0.252''/\text{pix}$ scale (pixel scale for a 1×1 binning).

In South America, we used the New Technology Telescope (NTT), located at La Silla Observatory (Chile), equipped with the ESO Faint Spectrograph and Camera (version 2) or EFOSC2 mounted at the Nasmyth B focus of the telescope. We observed in imaging mode with the R Bessel filter and a 2×2 binning mode. The camera is equipped with a 2048×2048 CCD with a pixel size of $15\times 15\mu\text{m}$ (pixel scale for a 1×1 binning). The field of view is $5.2'\times 5.2'$.

2.1.2 Regular program on lightcurves of TNOs

Usually, we studied short-term variability thanks to our program on lightcurves of KBOs at the Sierra Nevada Observatory (OSN) 1.5 m telescope. We present observations carried out at that telescope, at the 2.2 m and the 3.5 m Centro Astronomico Hispano Aleman (CAHA) telescopes at Calar Alto Observatory (Almeria, Spain) and at the 82 cm telescope of the Instituto de Astrofísica de Canarias (IAC-80 telescope) located at the Teide Observatory (Tenerife, Canary Islands, Spain).

The OSN observations were carried out by means of a $2\text{k}\times 2\text{k}$ CCD, with a total field of view of $7.8'\times 7.8'$. We used a 2×2 binning mode, which changes the image scale to $0.46''/\text{pixel}$ (pixel scale for a 2×2 binning).

For our CAHA observations, we used the Calar Alto Faint Object Spectrograph (CAFOS) at the 2.2 m telescope and the Large Area Imager for Calar Alto (LAICA) at the 3.5 m telescope. CAFOS is equipped with a 2048×2048 pixel CCD and image scale is $0.53''/\text{pixel}$ (pixel scale for a 1×1 binning). LAICA is equipped with a 2×2 mosaic of $4\text{k}\times 4\text{k}$ CCDs and its total field of view is $44.36'\times 44.36'$ and the pixel scale is $0.225''/\text{pixel}$.

We also present here a few observations carried out at the IAC-80 telescope. It is equipped with a $2\text{k}\times 2\text{k}$ CCD camera with a $13.5\times 13.5\mu\text{m}/\text{pixel}$ size (pixel scale for a 1×1 binning), installed at the Cassegrain primary focus. Its total field of view is $10.6'\times 10.6'$.

2.2 Observing strategy

Exposure times were chosen by considering two main factors. On one hand, it had to be long enough to achieve a signal-to-noise ratio (S/N) sufficient to study the observed object ($S/N > 20$). On the other hand, the exposure time had to be short enough to avoid elongated images of the target (when the telescope was tracked at sidereal speed) or elongated field stars (if the telescope was tracked at the TNO rate of motion). We always chose to track the telescope at sidereal speed. The drift rates of TNOs are typically low, $\sim 2''/\text{h}$, so exposure times around 300600 s were typically used.

The OSN, Calar Alto and IAC-80 observations reported in this work were performed without a filter in order to maximize the S/N. The main goal of our study is short-term variability via relative photometry. Therefore, the use of unfiltered images without absolute calibration is not a problem for our work. The R Bessel and R Johnson filters were used during our observations at the NTT and TNG, respectively. These filters were chosen to maximize the S/N on TNOs while minimizing the fringing that appears at longer wavelengths on images from these instruments.

The targets of our regular programme are typically

brighter than 21 mag in V. During our coordinated campaign, we also had the opportunity to use 4 m class telescopes to observe fainter objects and select targets with visual magnitudes between 21 and 22.5 mag. Relevant geometric information about the observed objects on the dates of observations, the number of images and filters used is summarized in Table 1

3 DATA REDUCTION AND ANALYSIS

3.1 Data reduction

During most observing nights, a series of biases and flat-fields were obtained to correct the instrumental signature from the images. We thus created a median bias and a median flat-field frame for each night of observation. Care was taken not to use bias or flat-field frames that might be affected by observational or acquisition problems. The median flat-fields were assembled from twilight dithered images and the results were inspected for possible residuals from very bright saturated stars. The flat-field exposure times were always long enough to ensure that no shutter effect was present, so that a gradient or an artefact of some sort could be present in the corrected images. Each target image was bias subtracted and flat-fielded using the median bias and median flat-field of the observation night. If daily information about bias and/or flat-field was not available, we used the median bias and median flat-field of a former or subsequent night.

Relative photometry using between 6 and 25 field stars was carried out by means of DAOPHOT routines (Stetson 1987). Care was taken not to introduce spurious results due to faint background stars or galaxies in the aperture. No cosmic ray removal algorithms were used. We rejected images in which the target is affected by a cosmic ray hit or by a nearby star. We used common reduction software for photometry data reduction of all the images adjusting the details of the parameters to the specificity of each data set.

The choice of the aperture radius is important. We had to choose an aperture as small as possible to obtain the highest S/N by minimizing the contribution from the sky, but large enough to include most of the flux of the TNO. Typically, we repeated the measurement using a set of apertures with radii around the full width at half-maximum, and also adaptable aperture radius (aperture radius is varying according to the seeing conditions of each image, and so, the aperture radius is different for each image). Then, we have to consider two factors in order to choose the best data reduction: the aperture size and the reference stars used. For all apertures used, we chose the results giving the lowest scatter in the photometry of both targets and stars. Several sets of reference stars were used to establish the relative photometry of all the targets. In many cases, several stars had to be rejected from the analysis because they showed some variability. Finally, the set that gave the lowest scatter was used for the final result. The final photometry of our targets was computed by taking the median of all the light curves obtained with respect to each reference star. By applying this technique, spurious results were eliminated and the dispersion of photometry was improved.

During the observational campaigns, we tried to stick

to the same field of view, and therefore to the same reference stars, for each observed target. In some cases, due to the drift of the observed object, the field changed completely or partially. If the field changed completely, we used different reference stars for two or three subsets of nights in the entire run. If the field changed partially, we tried to keep the greatest number of common reference stars during the whole campaign. In the case of our coordinated campaign using two telescopes, we tried to observe the same field of view with both telescopes for any given target. In this way, we can use the same reference stars and do a better job in image processing and analysis.

When we combined data from several observing runs, we normalized the photometry data to their average because we did not have absolute photometry allowing us to link runs. By normalizing over the averages of several runs, we assume that a similar number of data points are in the upper and lower part of the curves. This may not be so if runs were only two or three nights long, which is not usually the case. We wish to emphasize that we normalized to the average of each run and not the average of each night

3.2 Absolute photometry

We computed approximate R magnitudes for a few images per object per observational run. Namely, we computed approximate magnitudes for the OSN data of 2004 NT₃₃ and for all observations of 2002 TC₃₀₂, 2002 TX₃₀₀, 2004 XA₁₉₂, and 2005 UQ₅₁₃. In order to obtain approximate R-magnitudes, we used USNO-B1 stars in the field of view as photometric references. Since the USNO-B1 magnitudes are not standard BVRI magnitudes and since we also did not use BVRI filters, we derived very approximate magnitudes, with typical uncertainties of ~ 0.4 mag.

During our observations at the TNG and at the NTT, the R Johnson and the R Bessel filters were used, respectively. We are able to report an absolute photometry of all the data carried out during the coordinated campaign.

For absolute photometry, each image was reduced using standard techniques of calibration, as presented in this section (bias subtraction and flat-field correction). During each night of observations, Landolt standard stars (Landolt 1992) were observed at different air masses in order to calculate the calibration parameters such as photometric zero-point and first-order extinction coefficients.

TNOs are very faint objects, so the choice of the aperture in order to calculate the flux, or magnitude, is important. In fact, the aperture must be big enough to collect all the flux of the target without introducing the contaminating flux of the background. We computed their fluxes using a small aperture and corrected for the flux loss by means of the aperture correction (Howell 1989; Stetson 1990). We used between 5 and 15 stars in each field of view in order to compute the aperture correction for each object. The object aperture radius varied between 3 and 5 pixels, depending on the brightness of the target and on the night conditions. We chose the aperture that gave the highest S/N for each object by computing the growth curve of some stars (Howell 1989; Stetson 1990).

3.3 Period-detection methods

The final time-series photometry of each target was inspected for periodicities by means of the Lomb technique (Lomb 1976) as implemented in Press et al. (1992), but we also checked results by means of several other time series analysis techniques, such as Phase Dispersion Minimization (PDM), and CLEAN technique (Foster 1995). Harris et al. (1989) method and its improvement described in Pravec, Sarounova, & Wolf (1996) was also used (hereafter called Pravec-Harris method).

As mentioned before, the reference stars were also inspected for short-term variability and we can thus be confident that no error has been introduced by the choice of reference stars. Finally, in order to measure the amplitudes of short-term variability, we performed Fourier fits to the data to determine the peak-to-peak amplitudes (or full amplitudes).

4 PHOTOMETRIC RESULTS

In this section, we present our short-term variability results summarized in Table 2. The Lomb periodograms and lightcurves for all objects are provided in Figure 1 to Figure 21. We plotted all lightcurves over two periods. Times for zero phase, without light time correction, are reported in Table 2. For each lightcurves, a Fourier Series is used to fit the photometric data. Error bars for the measurements are not shown on the plots for clarity but one-sigma error bars on the relative magnitudes are reported in the online version of Table 3. Absolute magnitudes are also provided in the online version of Table 3.

The following subsections are dedicated to the short-term variability of our targets. We organized our results according to the Gladman dynamical classification (Gladman, Marsden, & Vanlaerhoven 2008).

4.1 Classical objects

4.1.1 (275809) 2001 QY₂₉₇

The time base (time coverage between the first and the last image of the object) of the 2009 data from the NTT is around 10.2 h split in two nights. The time base of our 2010 data is shorter; 2.3 h in three nights of observations. For our 2009 data set, the Lomb periodogram, PDM and CLEAN techniques suggested a rotational period of around 5.8 h. The PravecHarris technique inferred a double rotational period around 11.6 h. Our 2010 data set is clearly too short for a period search.

The Lomb periodogram (Fig. 1) of our two data sets showed three groups of peaks: the first one, with the highest confidence level, suggested a rotational period of around 5.84 h, the second one around 4.61 h and the last one around 7.25 h. The CLEAN technique confirmed a periodic signature at 5.84 ± 0.34 h. However, PDM presented a single-peaked period of 7.21 ± 0.39 h, and the Pravec-Harris technique a period around 14.4 ± 0.6 h and a possible rotational period of 5.84 ± 0.34 h. The best-fitting lightcurve is obtained for a period of 5.84 h (Fig. 2) because the alternative fits show more scatter. The amplitude of the lightcurve is large, 0.49 ± 0.03 mag assuming a 5.84 h periodicity. Assuming that

large amplitudes (>0.15 mag) are mainly due to shape effects, we must consider the double-peaked lightcurve (see Section 5). Then, if 5.84 h is our preferred photometric period, a preferred rotational period of 11.68 h (2×5.84) is deduced.

To our knowledge, a previous study of this target, based on 13 images obtained in around 5 h of observations, was done by Kern (2006) who suggested a rotational period of 12.2 ± 4.3 h and an amplitude of 0.66 ± 0.38 mag. We conclude, in agreement with Kern (2006), that 2001 QY₂₉₇ has a moderately long rotational period and a very high amplitude.

We must point out that 2001 QY₂₉₇ has a satellite. This system is an asynchronous binary system because the primary has a much smaller rotational period than the orbital one. Both components of the system are not resolved in our data, so, we are measuring the magnitude of the pair. The satellite has a long orbital period: 138.11 ± 0.02 days and it is orbiting at a distance of 9960 ± 30 km from the primary (Grundy et al. 2011). The magnitude difference between 2001 QY₂₉₇ and its satellite is 0.42 ± 0.07 (Noll et al. 2008). Due to the orbital and physical characteristics of the system, the satellite contribution to the lightcurve is negligible.

4.1.2 (307251) 2002 KW₁₄

We observed this target along ~ 10 h during three nights at the NTT and 0.2 h at the TNG. The Lomb periodogram (Fig. 3) shows a peak with a high confidence level at 4.29 h (5.59 cycles/day) and two aliases, with a lower confidence level, at 5.25 h (4.57 cycles/day) and at 3.69 h (6.49 cycles/day). All the techniques used confirmed a photometric rotational period of 4.29 h or 5.25 h with a similar confidence level. Assuming that the lightcurve is essentially due to the shape of the target, we must consider the double peaked one: the rotational period of 2002 KW₁₄ should be 8.58 h or 10.5 h. Our preferred period is 8.58 h, corresponding to an amplitude of 0.21 ± 0.03 mag (Fig. 4). However, also a lightcurve fit assuming a rotational period of 10.5 h with an amplitude of 0.26 ± 0.03 mag is possible.

4.1.3 (55636) 2002 TX₃₀₀

The 2003 data set is already published in Thirouin et al. (2010) in which we concluded that the rotational period of this object should be 8.14 ± 0.02 h. Ortiz et al. (2004) published a rotational period of 7.89 ± 0.03 and Sheppard & Jewitt (2003) presented a 8.12 h or a 12.1 h single-peaked rotational lightcurve.

In Fig. 5, we present the Lomb periodogram of all our dataset (2003, 2009, and 2010) with light-time correction. We note a peak with a high confidence level at 4.08 h (5.89 cycles/day). All used techniques confirmed this period, except Pravec-Harris method which favored a double peaked period at 8.15 h (2.94 cycles/day). A double peaked lightcurve seems to be the best option and it is presented in Fig. 6. However, the possibility of a rotational period around 12 h cannot be excluded. The corresponding amplitude is 0.05 ± 0.01 mag in all cases. More data are needed to confirm one of these two possible rotational periods. Due

to the low-amplitude lightcurve of 2002 TX₃₀₀, very high quality of data is needed.

4.1.4 2004 NT₃₃

We have a time base of ~ 16 h at the TNG during three nights and of 19.5 h at the OSN over six nights. The Lomb periodogram (Fig. 7) shows a peak with a high confidence level at 7.87 h (3.05 cycles/day) and two aliases with a lower confidence level at 11.76 h (2.04 cycles/day) and at 5.91 h (4.06 cycles/day). PDM, and CLEAN techniques confirmed the highest peak around 7.8 h. The Pravec-Harris technique suggested a rotational period of 7.87 h, a double-peaked period of 23.52 h, and a possible rotational period of 3.1 h (7.74 cycles/day). The best-fitting lightcurve is obtained for a period of 7.87 h and a corresponding amplitude of 0.04 ± 0.01 mag (Fig. 8).

4.1.5 (230965) 2004 XA₁₉₂

We have more than 18 h of observation in seven nights in October and more than 7 h during one night in December. The Lomb periodogram (Fig. 9) shows two peaks with a similar confidence level. The second peak at 7.88 h (3.05 cycles/day) seems to be a little bit higher than the first one at 11.49 h (2.09 cycles/day). PDM and CLEAN techniques confirmed the second peak at 7.88 h, but a period around 11 h is still present with a high confidence level. The Pravec-Harris technique presented a double-peaked period at 15.76 h. In all cases, the amplitude of the curve is 0.07 ± 0.02 mag. A rotational period of 7.88 h appears to be the best option for this object (Fig. 10). The alternative fit of 11.49 h exhibits more scatter and should be probably discarded.

4.1.6 (202421) 2005 UQ₅₁₃

The time base of our August run is around 10 h. In September, the time base is 8 h split in three nights and in October, it is around 45 h in six nights. The Lomb periodogram (Fig. 11) showed one clear peak and a possible 24h-alias. The highest peak is located at 7.03 h (3.41 cycles/day) and the second one is located at 10.01 h (2.40 cycles/day). In Fig. 12, we present both lightcurves. In all cases, the amplitude of the curve is 0.06 ± 0.02 mag. PDM, CLEAN, Pravec-Harris techniques confirmed these two peaks with a similar spectral power. There is no published photometry for this object, so we cannot compare our results and favor a clearly rotational period.

4.2 A resonant object

4.2.1 (84522) 2002 TC₃₀₂

It is in the 5:2 resonance with Neptune. Time base is, respectively, 10 h over 2 nights, 7 h over two nights and 0.5 h in one night. The Lomb periodogram (Fig. 13) presents three peaks with similar confidence levels. The highest peak is located at 5.41 h (4.44 cycles/day) and two aliases are found at 4.87 h (4.93 cycles/day) and at 6.08 h (3.95 cycles/day). PDM and Pravec-Harris techniques confirmed the highest peak at 5.41 h, but CLEAN favored a rotational period of 6.08 h. The best-fitting lightcurve is obtained for a rotational

period of 5.41 h. In Fig. 14, we present the single-peaked lightcurve with an amplitude of 0.04 ± 0.01 mag.

4.3 Scattered disc object (SDO) and detached disc objects

4.3.1 (40314) 1999 KR₁₆

It is a detached disc object. We have less than 30 images for this object, so we cannot present a satisfactory study based only on our data alone. We are just able to estimate an amplitude variation around 0.22 mag in 3.4 h of observations.

We found data that has been already published about 1999 KR₁₆¹. Using their 2001 data set, Sheppard & Jewitt (2002) obtained two best-fit periods of 5.840 h and 5.929 h, but they did not discard the possibility of a double-peaked period. We merged Sheppard & Jewitt (2002) data and our data in order to obtain an accurate lightcurve. The Lomb periodogram (Fig. 15) shows one peak with a high confidence level, located at 5.80 h (4.14 cycles/day) and two aliases at 7.73 h (3.10 cycles/day) and at 4.73 h (5.08 cycles/day). PDM and CLEAN techniques confirmed the rotational period of 5.8 h. Pravec-Harris method suggested the double-peaked period. In Fig. 16, we present the single-peaked lightcurve. The amplitude of the curve is 0.12 ± 0.06 mag, which is not at odds with Sheppard & Jewitt (2002), within uncertainty limits, even if slight differences can be seen, maybe due to the fact that usually Sheppard & Jewitt (2002) perform sinusoidal fits instead of the Fourier series method used in this work. We suggest a rotational period estimation of 5.8 h, close to the one estimated by Sheppard & Jewitt (2002) for this object.

4.3.2 (44594) 1999 OX₃

It is a scattered disc object. Time base of our data is around 14 h over three nights of observations. The Lomb periodogram (Fig. 17) shows several peaks. The highest one is found at 15.45 h (1.55 cycles/day). We note two aliases at 9.26 h (2.59 cycles/day) and at 36.92 h (0.65 cycles/day). The PDM technique favored the peak around 9 h. CLEAN shows two peaks with a similar confidence level around 9 h and 15 h. The Pravec-Harris method favored three possible rotational periods: 9.26 h, 13.4 h, and 15.45 h. In Fig. 18 and Fig. 19, we present all lightcurves. The amplitude of the curves is 0.11 ± 0.02 mag. To our knowledge, there is no published photometry for this object to compare with.

4.3.3 (145480) 2005 TB₁₉₀

It is a detached disc object. The Lomb periodogram (Fig. 20) shows one peak with a high confidence level and two aliases with a lower confidence level. The highest peak is located at 12.68 h (1.89 cycles/day) and the two aliases are located at 28.57 h (0.84 cycles/day) and at 8.16 h (2.94 cycles/day). All techniques confirm a rotational period of 12.68 h for this target, as shown in Fig. 21 for the single-peaked lightcurve.

¹ Rousselot, Petit, & Belskaya (2005) created a database in which lightcurves and photometric data of TNOs can be found (<http://www.obs-besancon.fr/bdp/>)

The Pravec-Harris technique favored two possible rotational periods: 12.68 h and 16.32 h (2×8.16 h). Our first estimation of 12.68 h seems to be the best option. The amplitude of the curve is 0.12 ± 0.01 mag.

5 DISCUSSION

The detached disc object, 2005 TB₁₉₀, is a paradigmatic example of the efficiency of having coordinated campaigns. In fact, during the first two nights, we managed to coordinate observations from the Canary Islands and Chile, observing this body on the first night during 2.2 h at the TNG, and around 4 h at the NTT, allowing us to study close to a half-period on one single coordinated night. Finally, with less than 50 images in 4 nights, we could reliably estimate the moderately long rotational period for this object. Detection and reliable estimations of long rotational periods were one of the goals of this coordinated campaign. We would have probably needed many more images and detection of this long periodicity would have probably been difficult without a coordinated campaign. Thus we consider our first coordinated campaign as a successful beginning.

As a general feature of our results, we report that the average amplitude of our sample is 0.13 mag. We note that in our 10 objects sample, only 2 have amplitudes larger than 0.15 mag. Thirouin et al. (2010) and Duffard et al. (2009) suggested a threshold of 0.15 mag in order to distinguish among lightcurve variations due to albedo or due to the shape of the target because the best fits to Maxwellian distributions were obtained with that assumption. Low amplitudes can be explained by albedo heterogeneity on the surface of a MacLaurin spheroid, while large amplitudes of variability are probably due to the shape of an elongated Jacobi body. According to this assumption, we introduce the criterion to consider that a high lightcurve amplitude of a large object may be attributed to a non spherical shape (typically a triaxial ellipsoid). In this case, we prefer the double peaked lightcurve to represent a complete rotation of the object. We must point out that to distinguish between shape and albedo contribution in a lightcurve is not trivial at all. In Table 2, we indicate the rotational periods obtained from data reduction (preferred photometric period) and the preferred rotational period assuming our criterion. For example, in the case of 2001 QY₂₉₇, our data analysis suggests a rotational period of 5.84 h, but given an amplitude larger than 0.15 mag, the amplitude variation is probably due to the shape of the object and we prefer the double peaked period, 11.68 h (2×5.84 h) as true rotational period of the object.

In Fig. 22, we plot the lightcurve peak-to-peak amplitude versus the absolute magnitude of results shown in this work and already published in Thirouin et al. (2010). As shown in Fig. 22, the majority of studied objects present a low amplitude, typically < 0.15 mag. In fact, except some cases like 2001 QY₂₉₇, most TNOs have a low amplitude. We found an average amplitude of 0.09 mag, 0.11 mag, 0.12 mag and 0.10 mag for, respectively, the scattered/detached, the resonant, the classical and the centaur groups. So, there is not a dynamical group with a higher/smaller amplitude in our database. We must point out that the lack of long rotational periods, previously mentioned in Thirouin et al. (2010) seems to be confirmed by this new work. In fact, ex-

cept 2005 TB₁₉₀ and probably 2001 QY₂₉₇, all our targets present a rotational period < 10 h.

Assuming TNOs in general as triaxial ellipsoids, with axes $a > b > c$ (rotating along c), the lightcurve amplitude, Δm , varies as a function of the observational angle ξ (the angle between the rotation axis and the line of sight) according to Binzel et al. (1989):

$$\Delta m = 2.5 \log \left(\frac{a}{b} \right) - 1.25 \log \left(\frac{a^2 \cos^2 \xi + c^2 \sin^2 \xi}{b^2 \cos^2 \xi + c^2 \sin^2 \xi} \right) \quad (1)$$

We computed a lower limit for the object elongation (a/b), assuming an equatorial view ($\xi = 90^\circ$)

$$\Delta m = 2.5 \log \left(\frac{a}{b} \right) \quad (2)$$

According to Chandrasekhar (1987) study of figures of equilibrium for fluid bodies, we can estimate lower limits for densities from rotational periods and the elongation of objects. That is to say, assuming that a given TNO is a triaxial ellipsoid in hydrostatic equilibrium (a Jacobi ellipsoid), we can compute a lower density limit. This study is summarized in Fig. 23 which is an update of fig. 7 of Duffard et al. (2009). In our sample, only two bodies have a high amplitude lightcurve (> 0.15 mag) and can be assumed to be Jacobi ellipsoids: 2001 QY₂₉₇ and 2002 KW₁₄. 2001 QY₂₉₇ has a very low density if it is in hydrostatic equilibrium and 2002 KW₁₄ seems to have a density between 0.5 and 1 g cm⁻³. Using Equation 1, we compute the lower limit for the densities of these two bodies, assuming a viewing angle of 60° ². The results are reported in Table 2. Most of our targets have low-amplitude lightcurves, probably due to albedo effects. So, they are probably MacLaurin spheroids and the study on lower limit densities cannot be applied. In fact, most of observed objects are far from the theoretical curves for acceptable values for the density which indicates that those objects are likely MacLaurin spheroids or are not in hydrostatic equilibrium (Fig. 23).

TNOs densities are an important physical characteristic. Unfortunately, their estimation is complicated and usually obtained just for binary and multiple systems. The range of published densities varies from around 1 g cm⁻³ for Varuna (Jewitt & Sheppard 2002) to 4.2 ± 1.3 g cm⁻³ for Quaoar (Fraser & Brown 2010) (however, a recent stellar occultation by Quaoar indicates that Quaoar density is probably much smaller than published one (Braga-Ribas et al. 2011)). Generally, densities are supposed to be very low in the Edgeworth-Kuiper Belt $\lesssim 1$ g cm⁻³, except for some “atypical” cases such as Haumea, Eris, and Pluto.

We also studied an asynchronous binary classical belt object, 2001 QY₂₉₇. We find a large lightcurve amplitude for this object, (0.49 ± 0.03) mag. A rotational period of 11.68 h seems to be the best candidate. The lightcurve of this object is likely due to its shape. Assuming that 2001 QY₂₉₇ is a triaxial ellipsoid in hydrostatic equilibrium, we estimate large axis ratios: b/a around 0.64 and c/a around 0.45.

If we assume that 2001 QY₂₉₇ is in hydrostatic equilibrium, we can estimate its bulk density, ρ , according to Chandrasekhar (1987), and define the volume of the system as $V_{sys} = M_{sys} / \rho$. Assuming that its rotational period is

² Given a random distribution of spin vectors, the average of viewing angle is 60° .

11.68 h, we estimate a lower limit density of $\rho=290 \text{ kg m}^{-3}$. Assuming that both components have the same albedo, we work out the primary radius by

$$R_{\text{primary}} = \left(\frac{3V_{\text{sys}}}{4\pi(1+10^{-0.6\Delta_{\text{mag}}})} \right)^{1/3} \quad (3)$$

where R_{primary} is the radius of the primary and Δ_{mag} is the component magnitude difference. Assuming that both components have the same albedo, we expressed the satellite radius as:

$$R_{\text{satellite}} = R_{\text{primary}} 10^{-0.2\Delta_{\text{mag}}} \quad (4)$$

with a $\Delta_{\text{mag}}=0.42$ (Noll et al. 2008) and a density, $\rho=290 \text{ kg m}^{-3}$, we computed a primary radius of 129 km and a satellite radius of 107 km for a total mass of the system, $M_{\text{sys}}=(4.105\pm0.038)\times10^{18} \text{ kg}$ (Grundy et al. 2011). The effective radius of the system is expressed as:

$$R_{\text{effective}} = \sqrt{R_{\text{primary}}^2 + R_{\text{satellite}}^2} \quad (5)$$

By using primary and secondary sizes obtained before, we computed an effective radius of 168 km for this system. We can derive the geometric albedo, p_{λ} , that is given by the equation:

$$p_{\lambda} = \left(\frac{C_{\lambda}}{R_{\text{effective}}} \right)^2 10^{-0.4H_{\lambda}} \quad (6)$$

C_{λ} is a constant depending on the wavelength (Harris 1998), and H is the absolute magnitude. The value we find for the geometric albedo is 0.08.

Assuming spherical shapes and densities between 500 and 2000 kg m^{-3} , Grundy et al. (2011) published an albedo range of 0.13–0.32. They also reported a primary radius ranging from 64 to 100 km (values obtained assuming spherical shapes and densities between 500 and 2000 kg m^{-3}). Due to the facts that 2001 QY₂₉₇ has a low inclination (1.5° , according to the Minor Planet Center (MPC) database) and a high albedo, Grundy et al. (2011) concluded that this body belongs to a more excited class of small TNOs (Brucker et al. 2009).

According to our study, 2001 QY₂₉₇ has instead a low albedo. Both studies, (Grundy et al. (2011) and our estimation) are preliminary, but *Herschel Space Observatory* key program “TNO’s are Cool!” estimated the albedo and the size of this binary object (Vilenius et al. 2012).

Various models can be enumerated in order to explain the formation of binary or multiple systems. Models based on gravitational capture have already been presented (Goldreich, Lithwick, & Sari 2002; Astakhov, Lee, & Farrelly 2005), as well as models based on low velocity collision between Kuiper Belt Objects (Durda et al. 2004) or the gravitational collapse model (Nesvorný, Youdin, & Richardson 2010). Recently, the possibility of rotational fission in the Kuiper Belt has been considered in Ortiz et al. (2012).

We computed the specific angular momentum of 2001 QY₂₉₇ system using the formula published in Descamps & Marchis (2008) and the scaled spin rate according to Chandrasekhar (1987). The specific angular momentum of this binary is 1.61 ± 0.13 and its scaled spin rate is 0.61 ± 0.01 (specific angular momentum and scaled spin rate are adimensional values). Those values seem to indicate that the 2001 QY₂₉₇ binary system was not formed by rotational fission. In fact,

the high value of the specific angular momentum and the scaled spin rate of this system do not fall into the “high size ratio binaries” region indicated in the fig. 1 of Descamps & Marchis (2008). So, we can probably discard a possible rotational fission origin for this binary. We cannot favor any other formation scenario; this system could have been formed by capture and/or collision, or gravitational collapse.

The last part of this section is dedicated to two examples of solar phase curves. The phase function can be expressed in flux as

$$\phi(\alpha) = 10^{-0.4\beta\alpha} \quad (7)$$

where α is the phase angle (in degrees) and β is the phase coefficient in magnitudes per degree at phase angles $<2^\circ$. All our targets were observed in a range of phase angles insufficient to perform a reliable study of the solar phase curve. Using various datasets already published, we report solar phase curves of (40314) 1999 KR₁₆ and of (44594) 1999 OX₃. Distance correction was applied and brightness variations due to rotation were removed to R-band magnitudes (R-band absolute magnitudes of TNG and NTT data in the online version of Table 3). Corrected R-band magnitudes will be called $m_R(1,1,\alpha)$ hereinafter, indicating with α the phase angle, “1” stands for 1 AU (geocentric and heliocentric distances). For observations done at the same phase angles, we averaged magnitudes and computed corresponding uncertainties.

In Fig. 24, we plot the solar phase curve of (40314) 1999 KR₁₆. According to Sheppard & Jewitt (2002) and to data reported in this work, we obtain a phase angle range of around 1.5° , $m_R(1,1,\alpha) = 5.41\pm0.03 \text{ mag}$ and $\beta = 0.12\pm0.03 \text{ mag-deg}^{-1}$. These results are consistent with Sheppard & Jewitt (2002), who found $m_R(1,1,\alpha) = 5.37\pm0.02 \text{ mag}$ and $\beta = 0.14\pm0.02 \text{ mag-deg}^{-1}$.

Fig. 25 shows the solar phase curve of (44594) 1999 OX₃, based on Bauer et al. (2003) and on our data. We get $m_R(1,1,\alpha) = 6.65\pm0.03 \text{ mag}$ and $\beta = 0.30\pm0.03 \text{ mag-deg}^{-1}$ from all data. Bauer et al. (2003) reported $m_R(1,1,\alpha) = 7.1 \text{ mag}$, uncorrected for phase angle and for possible rotation. Assuming albedo values of 0.25 and 0.05, we derived the conversion from $m_R(1,1,\alpha)$ to size, obtaining, respectively, size estimations of 130 and 300 km for 1999 OX₃. Assuming the same albedo values, we finally obtained a size range of 210–470 km for 1999 KR₁₆.

6 CONCLUSIONS

We have collected and analyzed R-band and Clear-band photometric data for TNOs in order to increase the number of objects studied so far. We have reported our first coordinated campaign for TNOs. Coordinating two telescopes, one in Chile and one in the Canary Islands allowed us to monitor during a long time our targets and to try to minimize aliases in the data analysis. We also report our latest result on short-term variability from our regular program of TNOs. We present a homogeneous dataset composed of 10 TNOs. Two of 10 objects (20 per cent) in our sample (2001 QY₂₉₇ and 2002 KW₁₄) show a lightcurve with an amplitude $\Delta_m \geq 0.15 \text{ mag}$. In an extended sample combining objects from this work and from Thirouin et al. (2010), we computed that 8 of 37 (22 per cent) targets have a

$\Delta_m \geq 0.15$ mag. Two of 10 objects (20 per cent) in our sample (2001 QY₂₉₇ and 2005 TB₁₉₀) have a rotational period $P_{rot} \geq 10$ h. In an extended sample combining objects from this work and from Thirouin et al. (2010), we computed that 5 of 37 (14 per cent) targets have a $P_{rot} \geq 10$ h. In fact, the sample of studied targets, in the literature, is highly biased toward objects with a short rotational period. The best option to debias the sample, and study objects with a medium to long rotational periodicity, is to carry out coordinated campaigns with two or three telescopes around the world.

In our sample, 80 per cent of the studied objects have a low variability (less than 0.15 mag) and corresponding lightcurves could be explained by albedo variations. Such bodies are probably MacLaurin spheroids. Just two of 10 objects (2001 QY₂₉₇ and 2002 KW₁₄) can be considered Jacobi ellipsoid with a high amplitude lightcurve, probably due to the shape of the body.

We also have studied a binary KBO which turned out to be asynchronous: 2001 QY₂₉₇ which presents a very high variability (> 0.4 mag) and a rotational periodicity longer than 10 h. Assuming that the system is in hydrostatic equilibrium and has a very low density, we derived a primary radius of 129 km, a secondary radius of 107 km and a geometric albedo of 0.08 for both components. We examined several possible formation scenarios. This binary was not likely formed by rotational fission due to its high specific angular momentum. We favor a collisional and/or capture scenario, however, a formation based on gravitational instability cannot be ruled out.

ACKNOWLEDGMENTS

We are grateful to the Sierra Nevada Observatory, Calar Alto, Telescopio Nazionale Galileo, New Technology Telescope, and El Teide Observatory staffs. This research was based on data obtained at the Observatorio de Sierra Nevada which is operated by the Instituto de Astrofísica de Andalucía, CSIC. This research is also based on observations collected at the Centro Astronómico Hispano Alemán (CAHA) at Calar Alto, operated jointly by the Max-Planck Institut für Astronomie and the Instituto de Astrofísica de Andalucía (CSIC). Other results were obtained at the Telescopio Nazionale Galileo. The Telescopio Nazionale Galileo (TNG) is operated by the Fundación Galileo Galilei of the Italian Istituto Nazionale di Astrofísica (INAF) on the island of La Palma in the Spanish Observatorio del Roque de los Muchachos of the Instituto de Astrofísica de Canarias. Some results are based on observations made with ESO New Technology Telescope (NTT) at the La Silla Observatory under programme ID 083.C-0642A. Some of the data published in this article were acquired with the IAC-80 telescope operated by the Instituto de Astrofísica de Canarias in the Observatorio del Teide. AT, JLO, NM, and RD were supported by AYA2008-06202-C03-01, and ACB was supported by AYA2008-06202-C03-03, which are Spanish MICINN and MEC projects. AT, JLO, NM, and RD also acknowledge the Proyecto de Excelencia de la Junta de Andalucía, J.A.2007-FQM2998. RD acknowledges financial support from the MICINN (Ramon y Cajal fellowship). FEDER funds are also acknowledged.

REFERENCES

- Astakhov S. A., Lee E. A., Farrelly D., 2005, *MNRAS*, 360, 401
- Bauer J. M., Meech K. J., Fernández Y. R., Pittichova J., Hainaut O. R., Boehnhardt H., Delsanti A. C., 2003, *Icar*, 166, 195
- Binzel R. P., Farinella P., Zappala V., Cellino A., 1989, *aste.conf*, 416
- Braga-Ribas F., et al., 2011, *epsc.conf*, 1060
- Brucker M. J., Grundy W. M., Stansberry J. A., Spencer J. R., Sheppard S. S., Chiang E. I., Buie M. W., 2009, *Icar*, 201, 284
- Chandrasekhar S., 1987, QB410,
- Descamps P., Marchis F., 2008, *Icar*, 193, 74
- Duffard R., Ortiz J. L., Thirouin A., Santos-Sanz P., Morales N., 2009, *A&A*, 505, 1283
- Durda D. D., Bottke W. F., Enke B. L., Merline W. J., Asphaug E., Richardson D. C., Leinhardt Z. M., 2004, *Icar*, 170, 243
- Fraser W. C., Brown M. E., 2010, *ApJ*, 714, 1547
- Foster G., 1995, *AJ*, 109, 1889
- Gladman B., Marsden B. G., Vanlaerhoven C., 2008, *ssbn.book*, 43
- Goldreich P., Lithwick Y., Sari R., 2002, *Natur*, 420, 643
- Grundy W. M., et al., 2011, *Icar*, 213, 678
- Harris A. W., et al., 1989, *Icar*, 77, 171
- Harris A. W., 1998, *Icar*, 131, 291
- Howell S. B., 1989, *PASP*, 101, 616
- Jewitt D. C., Sheppard S. S., 2002, *AJ*, 123, 2110
- Jewitt D., Luu J., 1993, *Natur*, 362, 730
- Kern S. D., 2006, *PhDT*,
- Landolt A. U., 1992, *AJ*, 104, 340
- Lomb N. R., 1976, *Ap&SS*, 39, 447
- Press W. H., Teukolsky S. A., Vetterling W. T., Flannery B. P., 1992, *nrfa.book*,
- Nesvorný D., Youdin A. N., Richardson D. C., 2010, *AJ*, 140, 785
- Noll K. S., Grundy W. M., Chiang E. I., Margot J.-L., Kern S. D., 2008, *ssbn.book*, 345
- Ortiz J. L., Gutiérrez P. J., Casanova V., Sota A., 2003, *A&A*, 407, 1149
- Ortiz J. L., et al., 2004, *A&A*, 420, 383
- Ortiz J. L., Gutiérrez P. J., Santos-Sanz P., Casanova V., Sota A., 2006, *A&A*, 447, 1131
- Ortiz J. L., Santos Sanz P., Gutiérrez P. J., Duffard R., Aceituno F. J., 2007, *A&A*, 468, L13
- Ortiz J. L., et al., 2012, *MNRAS*, 419, 2315
- Pravec P., Sarounova L., Wolf M., 1996, *Icar*, 124, 471
- Rousselot P., Petit J., Belskaya I., 2005, Abstract presented at Asteroids, Comets, Meteors.
- Sheppard S. S., Jewitt D. C., 2002, *AJ*, 124, 1757
- Sheppard S. S., Jewitt D. C., 2003, *EM&P*, 92, 207
- Sheppard S. S., Lacerda P., Ortiz J. L., 2008, *ssbn.book*, 129
- Stetson P. B., 1987, *PASP*, 99, 191
- Stetson P. B., 1990, *PASP*, 102, 932
- Thirouin A., Ortiz J. L., Duffard R., Santos-Sanz P., Aceituno F. J., Morales N., 2010, *A&A*, 522, A93
- Vilenius, E., Kiss, C., Mommert, M., et al., 2012, *A&A*, 541, A94

Table 1: Dates (UT-dates), heliocentric (r_h), and geocentric (Δ) distances and phase angle (α) of the observations. We also indicate the number of images used for this work and the number of taken images. For example, 1/5 indicates that 5 images were taken during our run but just 1 was used for this work. We also summarized the filter used and the telescope for each observational run.

Object	Date	# Images	r_h [AU]	Δ [AU]	α [deg]	Filter	Telescope
1999 KR ₁₆	26/07/2009	12/16	36.034	35.913	1.61	R	NTT
	27/07/2009	7/12	36.034	35.929	1.61	R	NTT
1999 OX ₃	25/07/2009	16/18	22.433	21.545	1.29	R	NTT
	26/07/2009	11/23	22.431	21.536	1.25	R	NTT
2001 QY ₂₉₇	27/07/2009	15/19	22.430	21.527	1.21	R	NTT
	24/07/2009	2/5	43.142	42.168	0.39	R	TNG
	24/07/2009	16/22	43.142	42.168	0.38	R	NTT
	25/07/2009	10/10	43.143	42.166	0.36	R	NTT
	05/08/2010	10/10	43.223	42.215	0.15	R	NTT
	13/08/2010	6/7	43.225	42.212	0.04	R	NTT
	14/08/2010	6/6	43.225	42.213	0.06	R	NTT
	24/07/2009	3/3	40.655	40.149	1.25	R	TNG
2002 KW ₁₄	25/07/2009	11/16	40.656	40.167	1.26	R	NTT
	26/07/2009	17/18	40.656	40.182	1.27	R	NTT
	27/07/2009	14/16	40.657	40.197	1.28	R	NTT
2002 TC ₃₀₂	15/10/2009	13/15	46.552	45.589	0.32	Clear	2.2 m Calar Alto telescope
	17/10/2009	19/21	46.551	45.582	0.28	Clear	2.2 m Calar Alto telescope
	09/09/2010	22/23	46.331	45.684	0.96	Clear	OSN
	11/09/2010	10/11	46.329	45.656	0.93	Clear	OSN
	01/12/2010	6/6	46.275	45.463	0.70	Clear	IAC-80
2002 TX ₃₀₀	07/08/2003	116/127	40.825	40.303	1.23	Clear	OSN
	08/08/2003	165/177	40.825	40.291	1.22	Clear	OSN
	09/08/2003	132/173	40.825	40.278	1.20	Clear	OSN
	18/10/2009	14/19	41.534	40.615	0.54	Clear	2.2 m Calar Alto telescope
	06/09/2010	9/14	41.639	40.901	0.95	Clear	OSN
	07/09/2010	4/7	41.639	40.891	0.94	Clear	OSN
	08/09/2010	25/25	41.639	40.884	0.92	Clear	OSN
	09/09/2010	13/19	41.640	40.875	0.91	Clear	OSN
	10/09/2010	34/36	41.640	40.867	0.90	Clear	OSN
	11/09/2010	5/5	41.640	40.857	0.88	Clear	OSN
2004 NT ₃₃	25/07/2009	14/14	38.164	37.327	0.87	R	TNG
	26/07/2009	11/11	38.164	37.234	0.87	R	TNG
	27/07/2009	11/21	38.164	37.321	0.86	R	TNG
	13/10/2009	15/15	38.185	37.783	1.38	Clear	OSN
	14/10/2009	19/20	38.185	37.796	1.39	Clear	OSN
	15/10/2009	15/15	38.185	37.810	1.39	Clear	OSN
	16/10/2009	12/15	38.186	37.824	1.40	Clear	OSN
	17/10/2009	15/20	38.186	37.837	1.41	Clear	OSN
	18/10/2009	10/20	38.186	37.851	1.41	Clear	OSN
	13/10/2009	12/12	35.799	35.507	1.53	Clear	OSN
2004 XA ₁₉₂	14/10/2009	6/10	35.799	35.494	1.52	Clear	OSN
	15/10/2009	10/10	35.799	35.481	1.52	Clear	OSN
	16/10/2009	10/10	35.799	35.467	1.51	Clear	OSN
	17/10/2009	22/24	35.799	35.454	1.50	Clear	OSN
	18/10/2009	13/13	35.798	35.439	1.49	Clear	OSN
	17/12/2009	31/33	35.787	34.978	0.91	R	3.5 m Calar Alto telescope
2005 TB ₁₉₀	24/07/2009	6/6	46.396	45.650	0.86	R	TNG
	24/07/2009	10/24	46.396	45.650	0.86	R	NTT
	25/07/2009	7/11	46.396	45.638	0.84	R	TNG
	25/07/2009	5/8	46.396	45.638	0.84	R	NTT
	26/07/2009	8/8	46.396	45.627	0.82	R	TNG
	27/07/2009	12/12	46.396	45.616	0.81	R	TNG
2005 UQ ₅₁₃	02/08/2008	5/10	48.806	48.389	1.09	Clear	OSN
	03/08/2008	7/13	48.806	48.376	1.08	Clear	OSN

04/08/2008	13/15	48.806	48.362	1.07	Clear	OSN
09/08/2008	20/25	48.805	48.294	1.03	Clear	OSN
20/09/2009	15/18	48.735	47.859	0.58	Clear	OSN
21/09/2009	38/41	48.735	47.855	0.57	Clear	OSN
23/09/2009	18/19	48.735	47.847	0.55	Clear	OSN
13/10/2009	33/35	48.731	47.826	0.50	Clear	OSN
14/10/2009	30/35	48.731	47.828	0.50	Clear	OSN
15/10/2009	30/30	48.731	47.830	0.51	Clear	OSN
16/10/2009	24/25	48.731	47.832	0.51	Clear	OSN
17/10/2009	31/35	48.731	47.834	0.52	Clear	OSN
18/10/2009	10/14	48.731	47.837	0.52	Clear	OSN

Table 2. Summary of results from this work. In this table, we present the name of the object, the preferred period (Pref. rot. per. in hour), the preferred photometric period (Pref. phot. per. in hour) and lightcurve amplitude (Amp. in magnitude), the Julian Date (φ_0) for which the phase is zero in our lightcurves (without light time correction), and the absolute magnitudes (Abs. mag.) (Absolute magnitudes extracted from the MPC database). Lower limit to the densities are also shown for two objects (see text). The preferred photometric period is the periodicity obtained thanks to the data reduction. In some cases, as mentioned in the Photometric Results and Discussion sections, we preferred the double rotational periodicity due to the high amplitude lightcurve (the preferred period). Zero phase of (40314) 1999 KR₁₆ extracted from Sheppard & Jewitt (2002).

Object	Pref. phot. per. [h]	Pref. rot. per. [h]	Amp. [mag.]	φ_0 [JD]	Abs. mag.	ρ [g/cm ³]
(40314) 1999 KR ₁₆	5.8	5.8	0.12±0.06	2451662.9409	5.8	
(44594) 1999 OX ₃	9.26 or 13.4 or 15.45	9.26 or 13.4 or 15.45	0.11±0.02	2455038.69404	7.4	
(275809) 2001 QY ₂₉₇	5.84	11.68	0.49±0.03	2455037.61147	5.7	0.29
(307251) 2002 KW ₁₄	4.29 or 5.25	8.58 or 10.5	(0.21 or 0.26)±0.03	2455037.40786	5.0	0.53 or 0.35
(84522) 2002 TC ₃₀₂	5.41	5.41	0.04±0.01	2455120.41362	3.8	
(55636) 2002 TX ₃₀₀	8.15 or 11.7	8.15 or 11.7	0.05±0.01	2452859.51500	3.3	
2004 NT ₃₃	7.87	7.87	0.04±0.01	2455038.48984	4.4	
(230965) 2004 XA ₁₉₂	7.88	7.88	0.07±0.02	2455118.50584	4.0	
(145480) 2005 TB ₁₉₀	12.68	12.68	0.12±0.01	2455037.62904	4.7	
(202421) 2005 UQ ₅₁₃	7.03 or 10.01	7.03 or 10.01	0.06±0.02	2455118.32179	3.4	

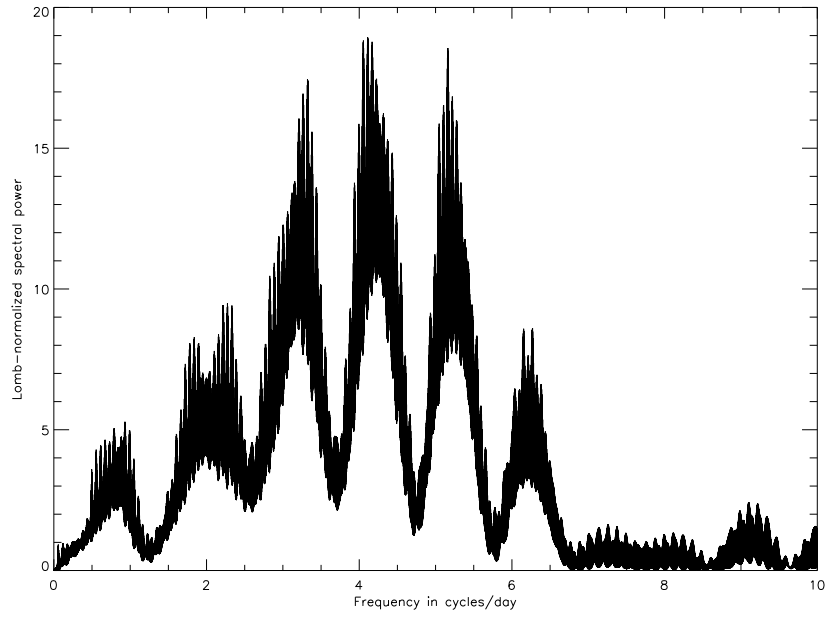


Figure 1. Lomb periodogram of 2001 QY₂₉₇

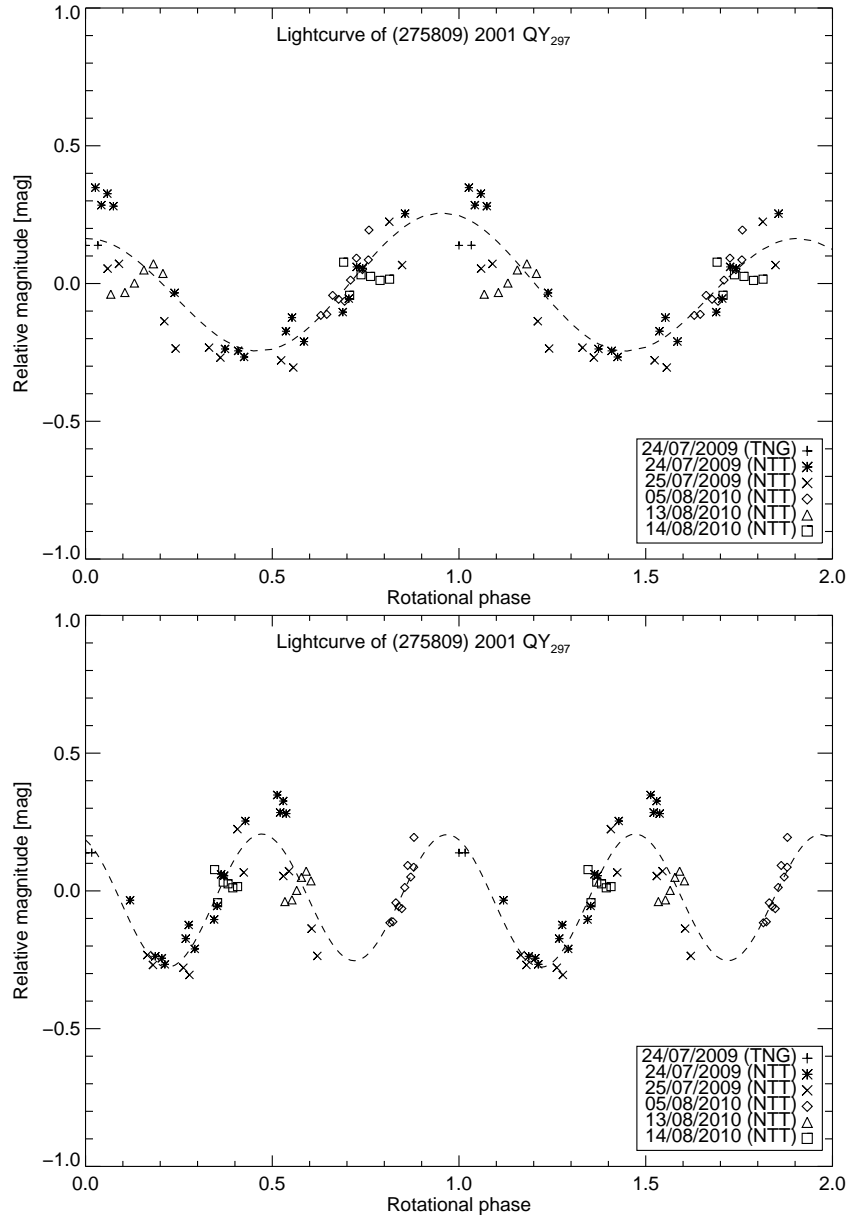


Figure 2. Rotational phase curves for 2001 QY₂₉₇ obtained by using a spin period of 5.84 h (upper plot) and 11.68 h (lower plot). The dash line is a Fourier Series fit of the photometric data. Different symbols correspond to different dates.

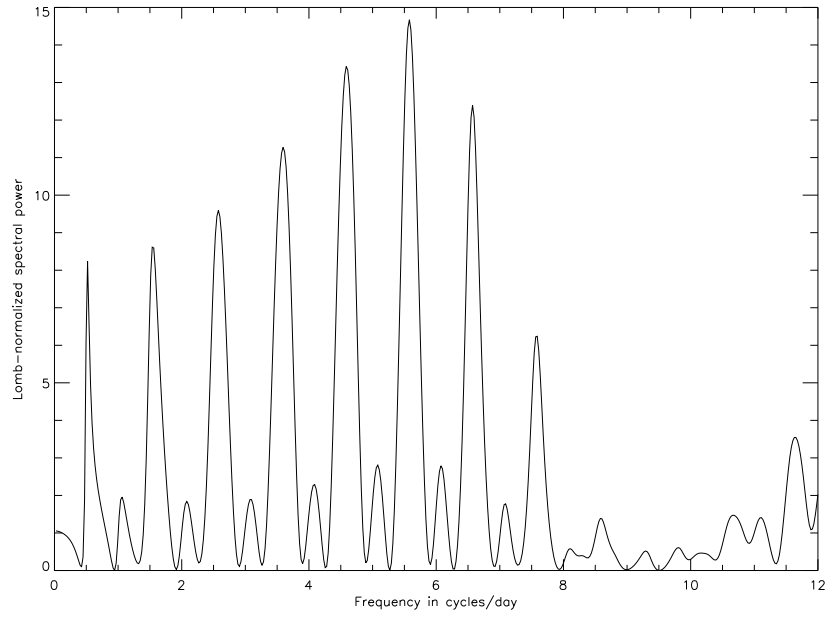


Figure 3. Lomb periodogram of 2002 KW₁₄

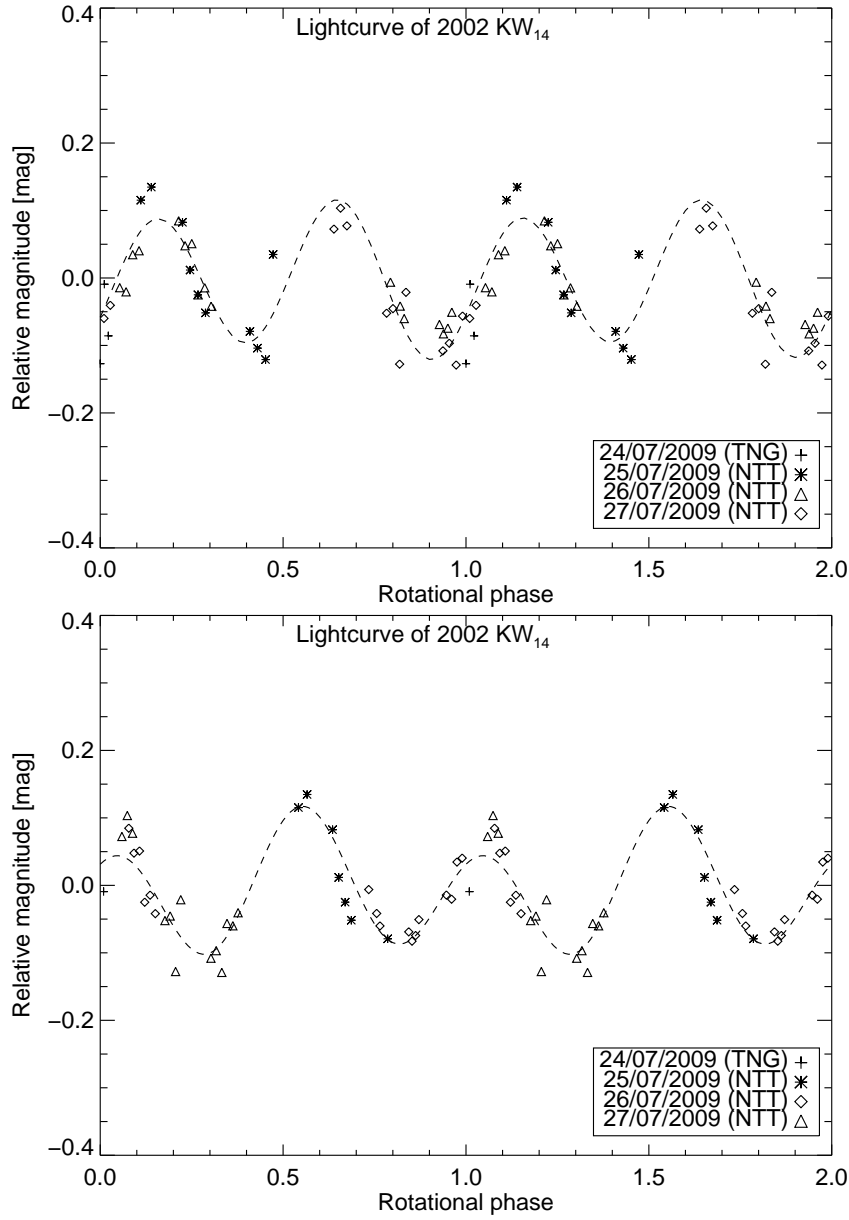


Figure 4. Rotational phase curves for 2002 KW₁₄ obtained by using a spin period of 8.58 h (upper plot) and 10.50 h (lower plot). The dash line is a Fourier Series fit of the photometric data. Different symbols correspond to different dates.

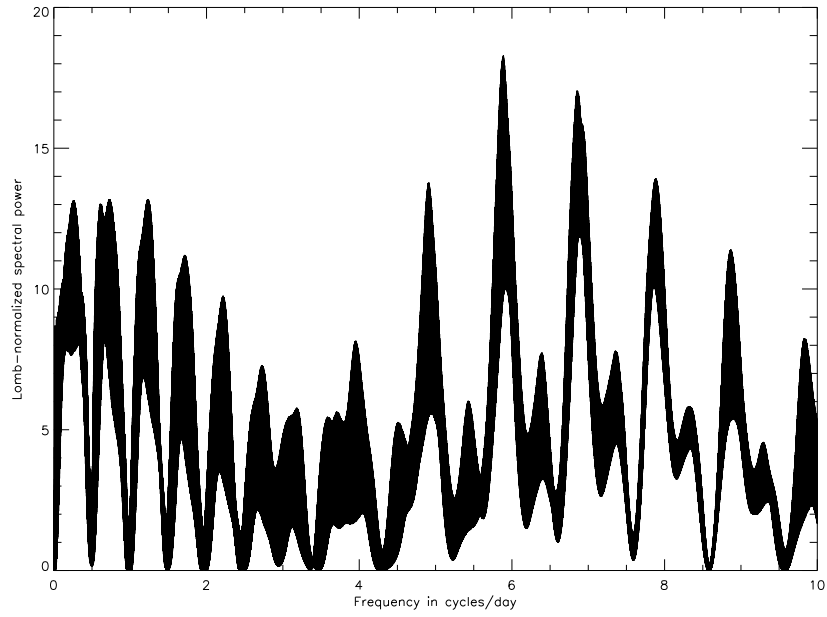


Figure 5. Lomb periodogram of 2002 TX₃₀₀

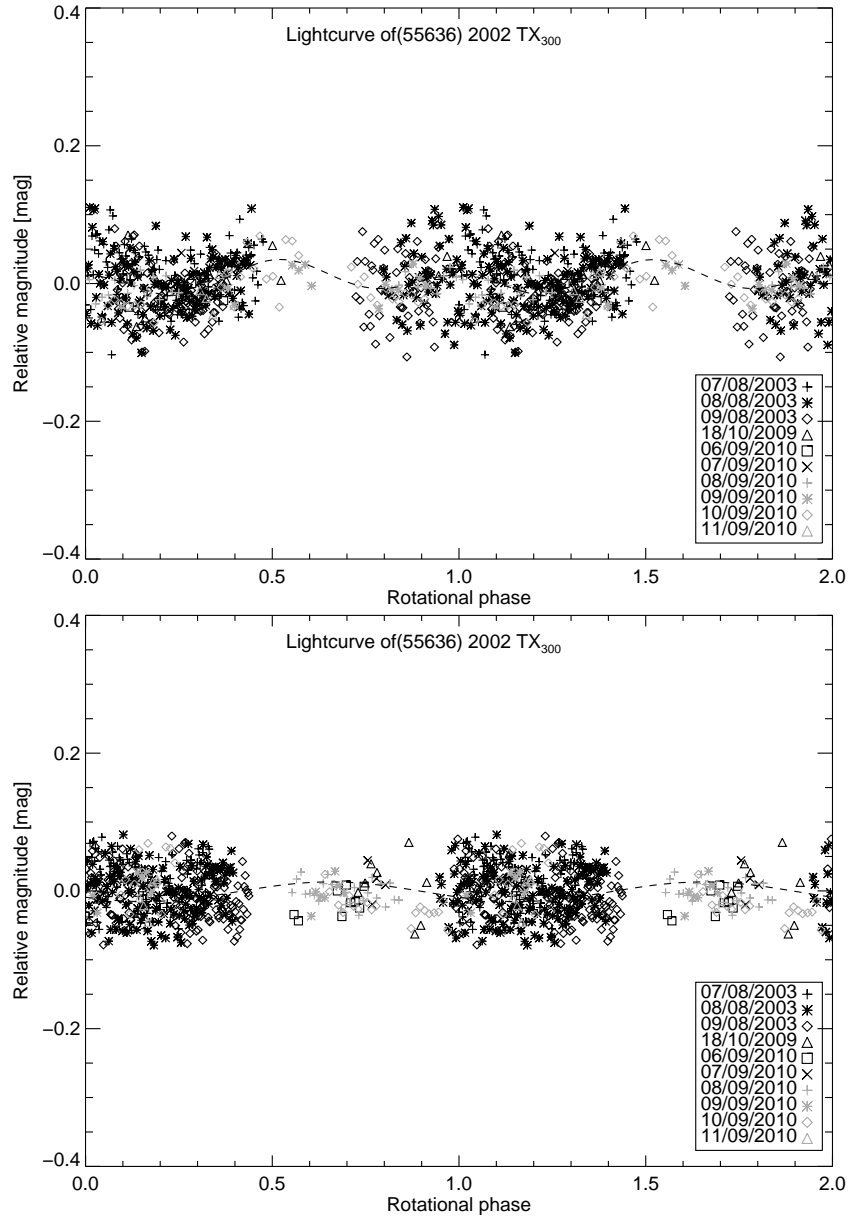


Figure 6. Rotational phase curves for 2002 TX₃₀₀ obtained by using a spin period of 8.15 h (upper plot) and 11.7 h (lower plot). The dash line is a Fourier Series fit of the photometric data. Different symbols correspond to different dates.

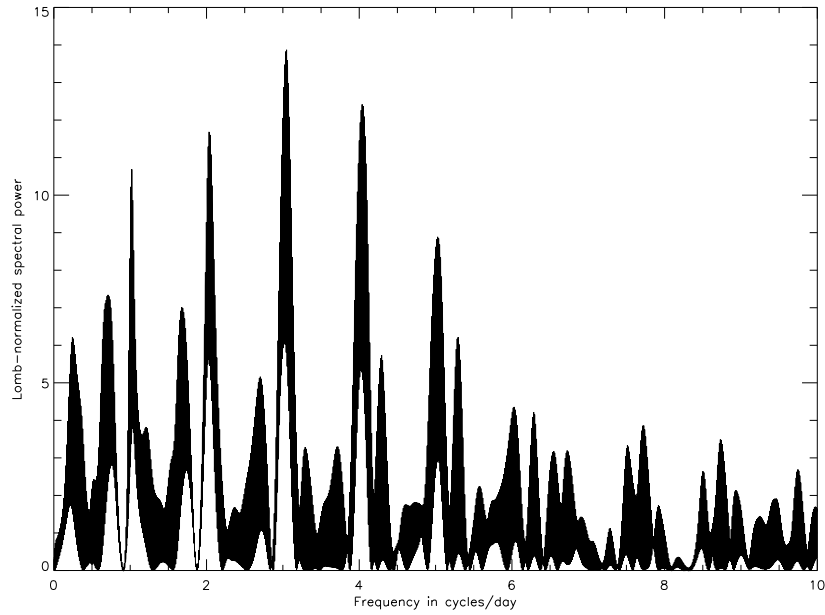


Figure 7. Lomb periodogram of 2004 NT₃₃

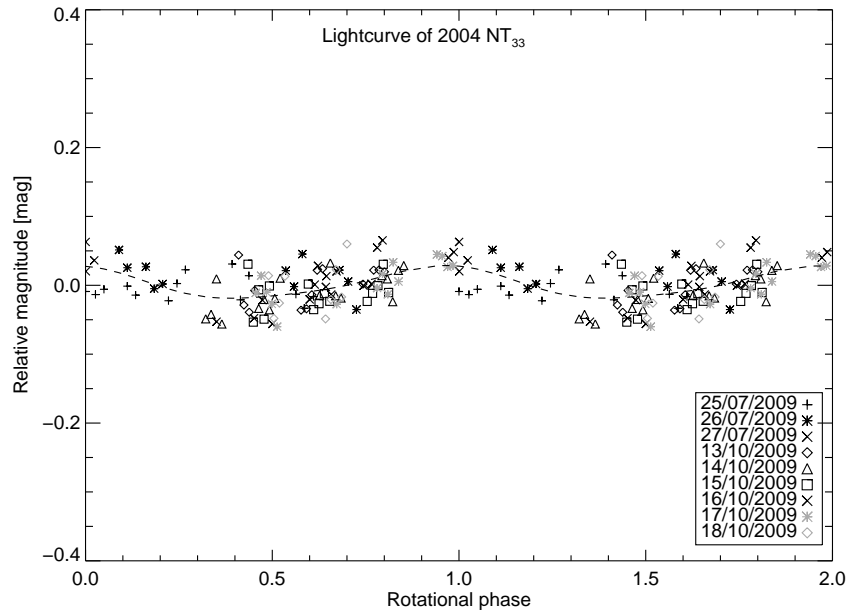


Figure 8. Rotational phase curves for 2004 NT₃₃ obtained by using a spin period of 7.87 h. The dash line is a Fourier Series fit of the photometric data. Different symbols correspond to different dates.

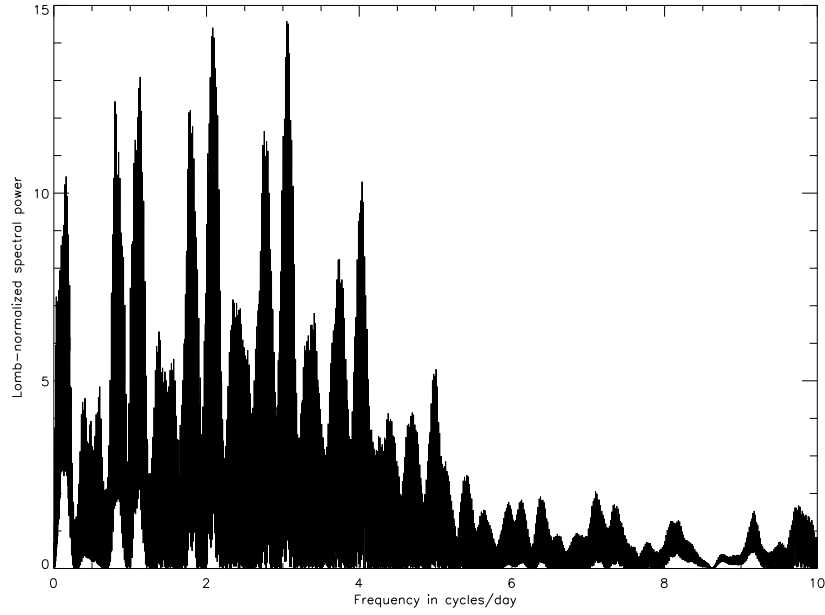


Figure 9. Lomb periodogram of 2004 XA₁₉₂

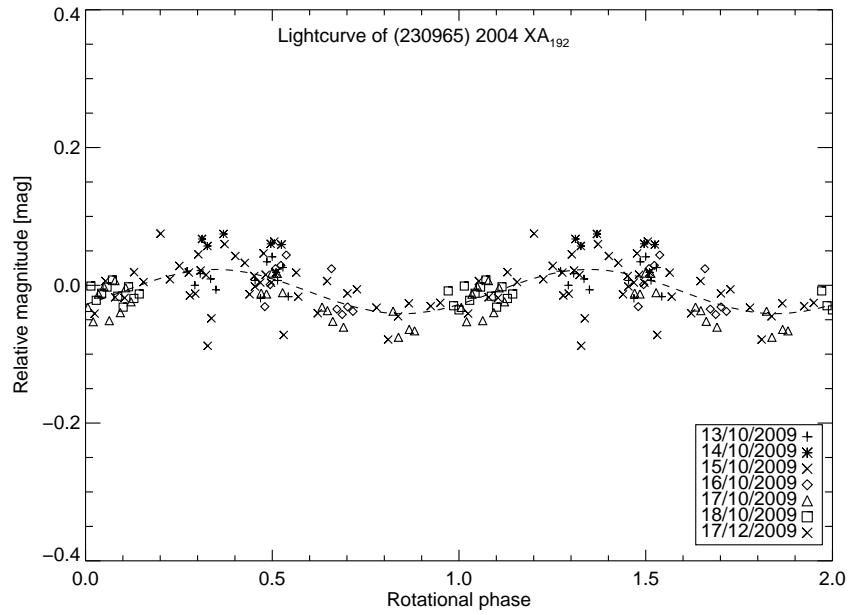


Figure 10. Rotational phase curve for 2004 XA₁₉₂ obtained by using a spin period of 7.88 h. The dash lines are a Fourier Series fits of the photometric data. Different symbols correspond to different dates.

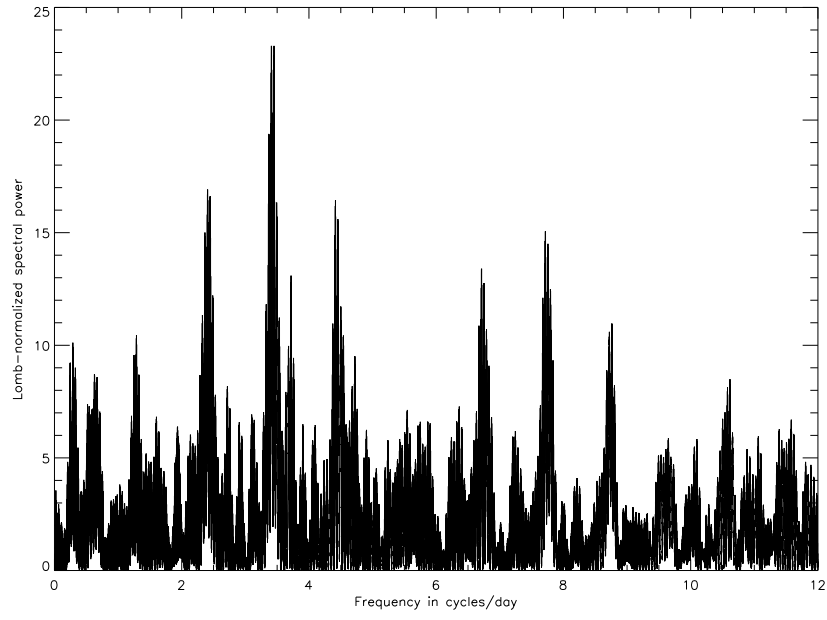


Figure 11. Lomb periodogram of 2005 UQ₅₁₃

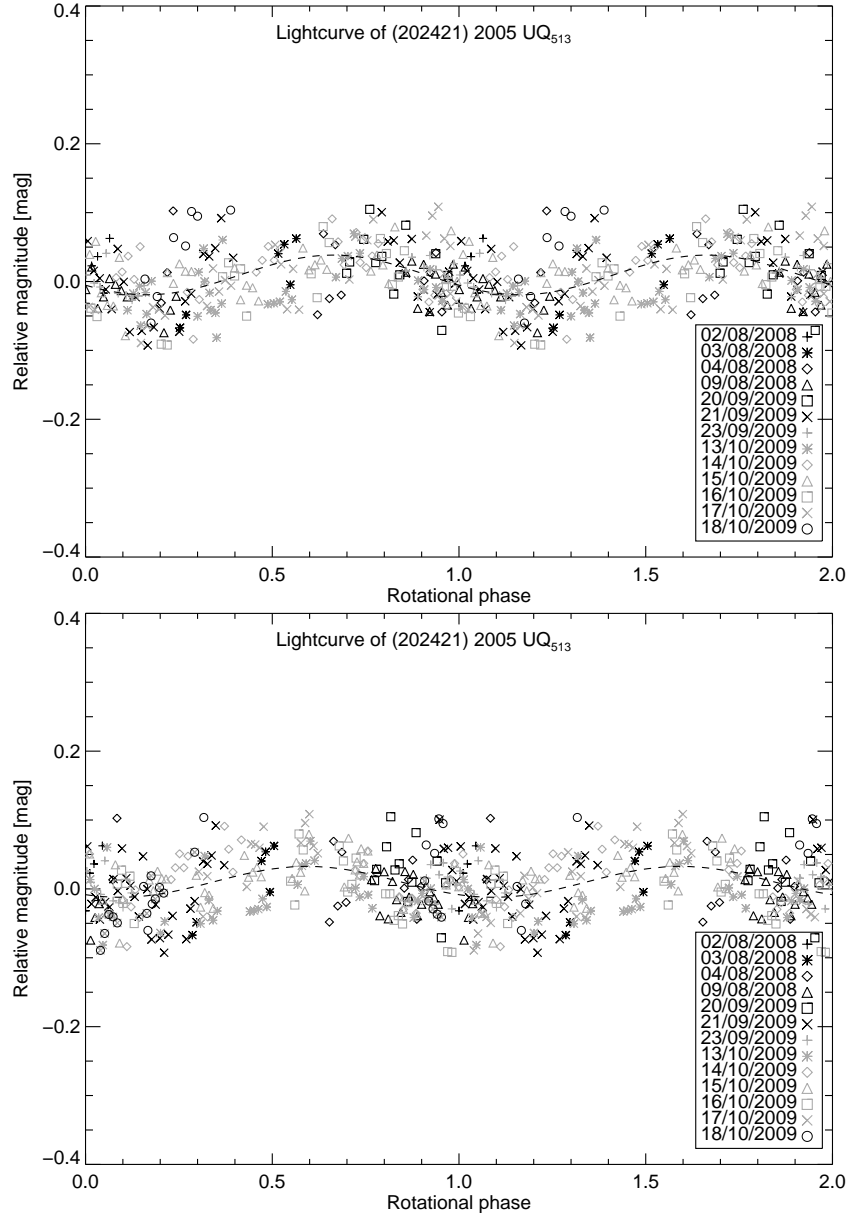


Figure 12. Rotational phase curves for 2005 UQ₅₁₃ obtained by using a spin period of 7.03 h (upper plot) and 10.01 h (lower plot). The dash line is a Fourier Series fit of the photometric data. Different symbols correspond to different dates.

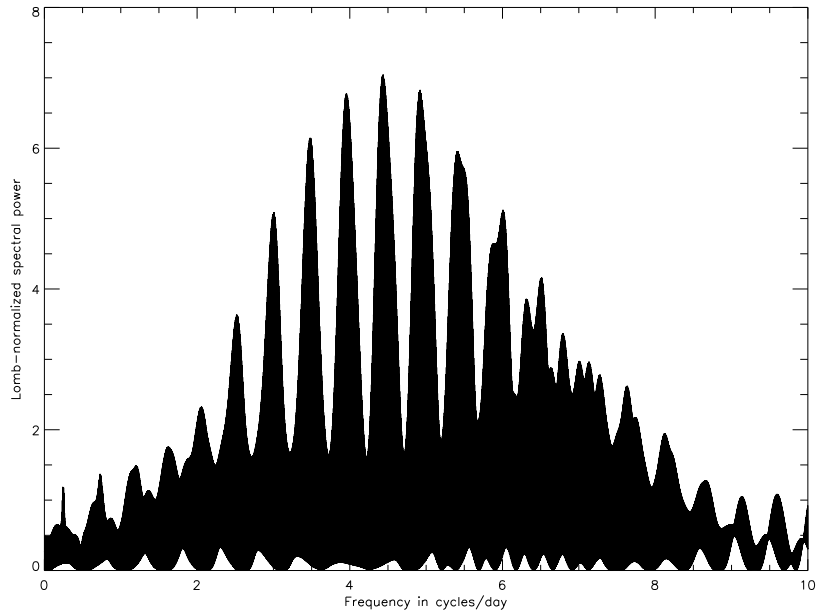


Figure 13. Lomb periodogram of 2002 TC₃₀₂

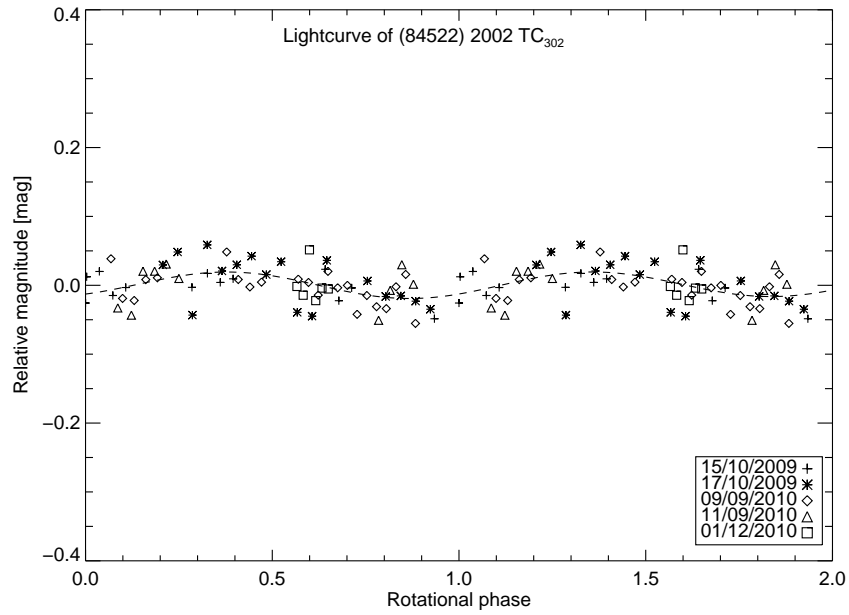


Figure 14. Rotational phase curve for 2002 TC₃₀₂ obtained by using a spin period of 5.41 h. The dash line is a Fourier Series fit of the photometric data. Different symbols correspond to different dates.

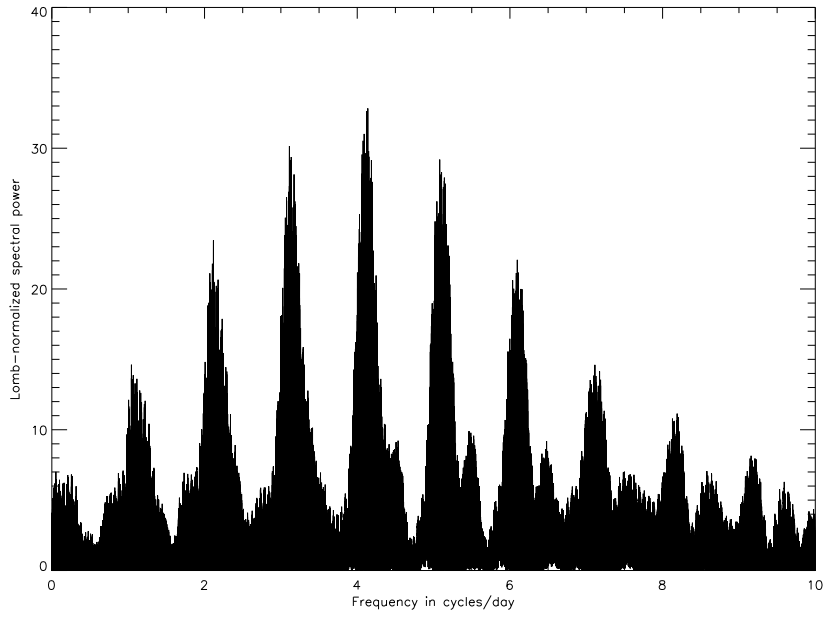


Figure 15. Lomb periodogram of 1999 KR₁₆

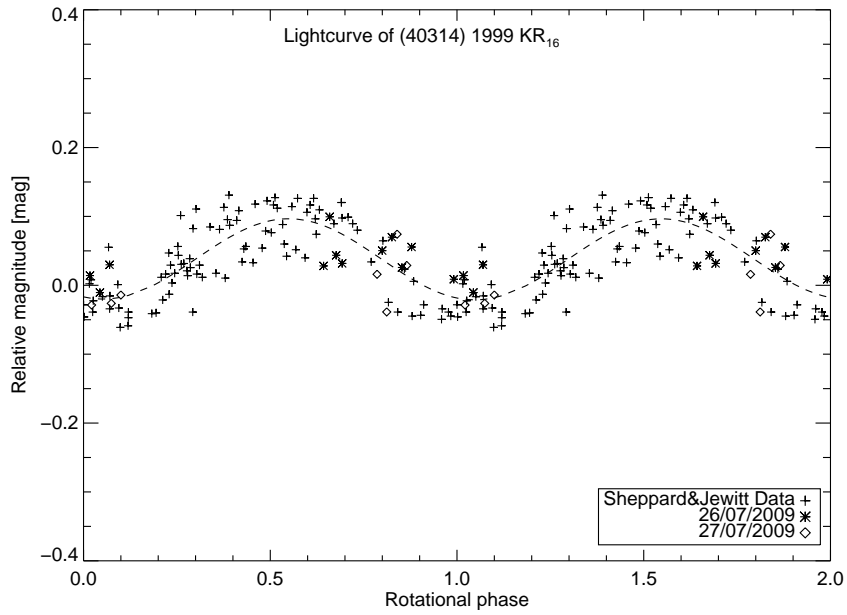


Figure 16. Rotational phase curve for 1999 KR₁₆ obtained by using a spin period of 5.8 h. The dash line is a Fourier Series fit of the photometric data. Different symbols correspond to different dates.

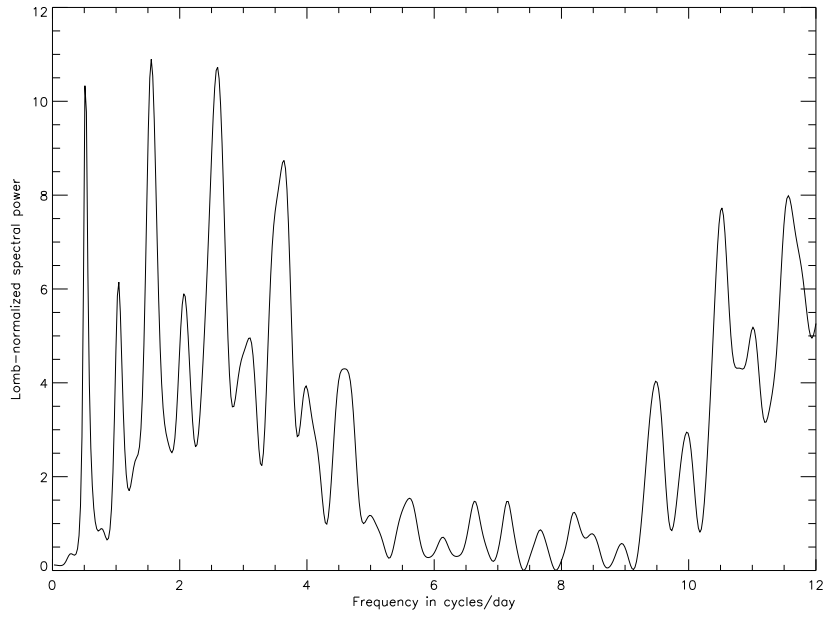


Figure 17. Lomb periodogram of 1999 OX₃

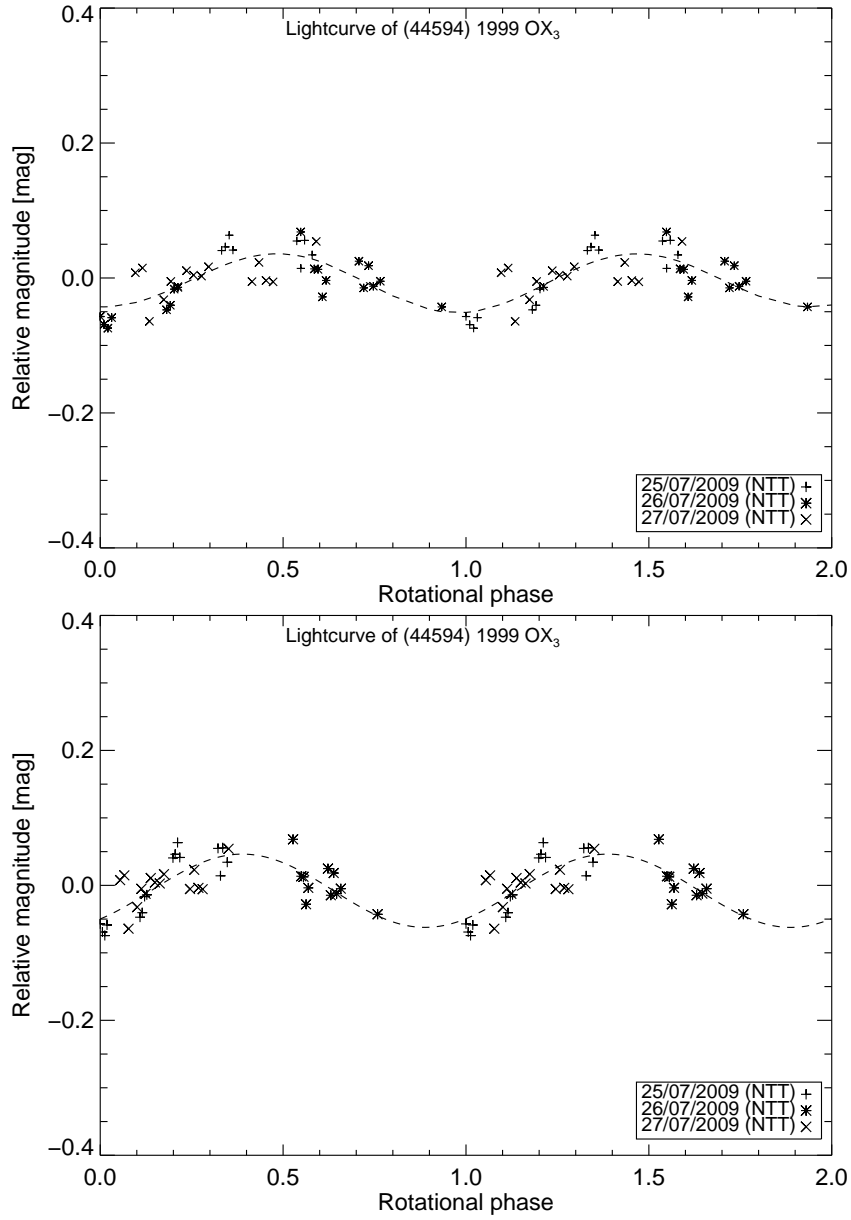


Figure 18. Rotational phase curves for 1999 OX₃ obtained by using different spin periods; 9.26 h (upper plot) and 15.45 h (lower plot). In both cases, we present a single peak lightcurve. The dash lines are a Fourier Series fits of the photometric data. Different symbols correspond to different dates.

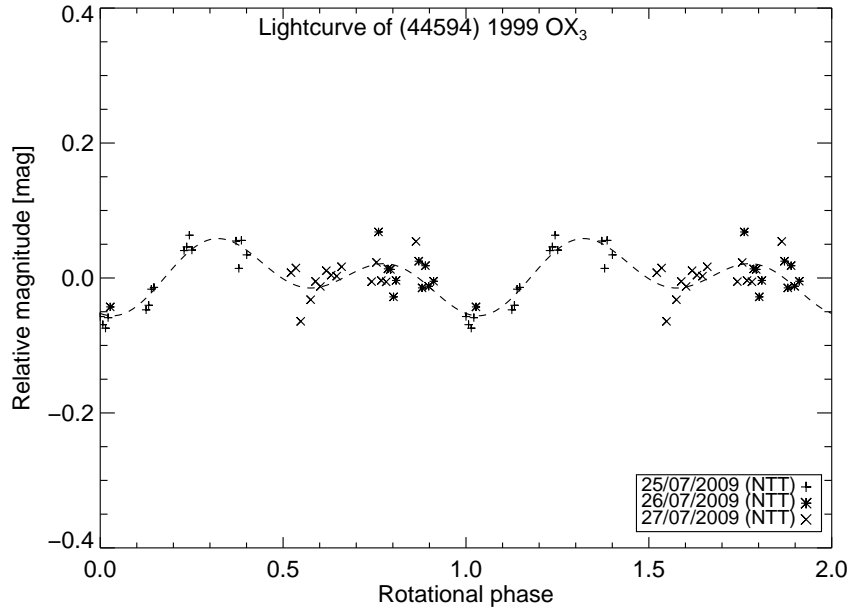


Figure 19. Rotational phase curves for 1999 OX₃ obtained by using a rotational period of 13.4 h. The dash lines are a Fourier Series fits of the photometric data. Different symbols correspond to different dates.

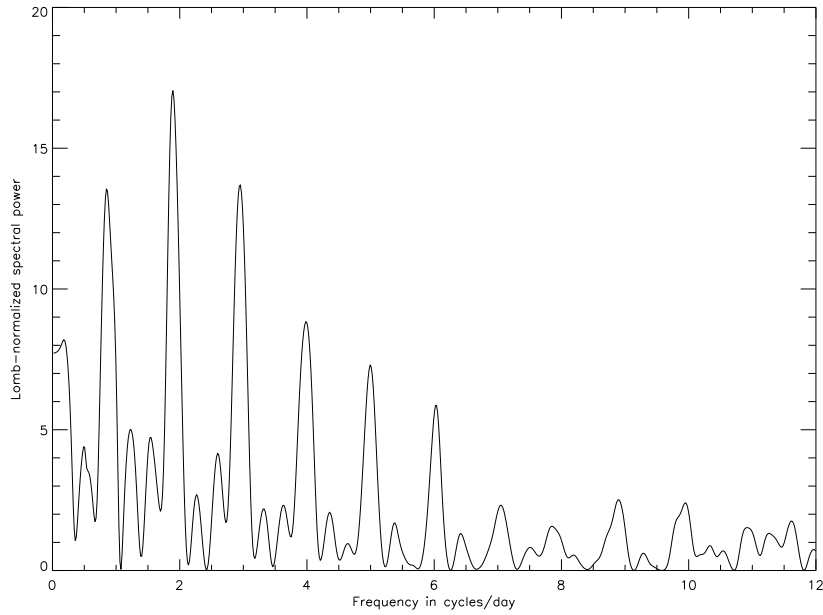


Figure 20. Lomb periodogram of 2005 TB₁₉₀

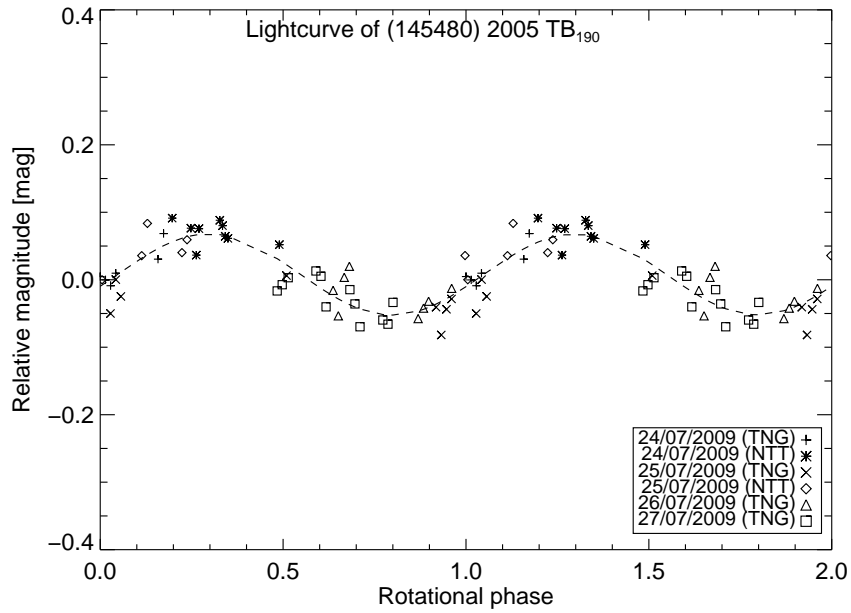


Figure 21. Rotational phase curve for 2005 TB₁₉₀ obtained by using a spin period of 12.68 h. The dash lines are a Fourier Series fits of the photometric data. Different symbols correspond to different dates.

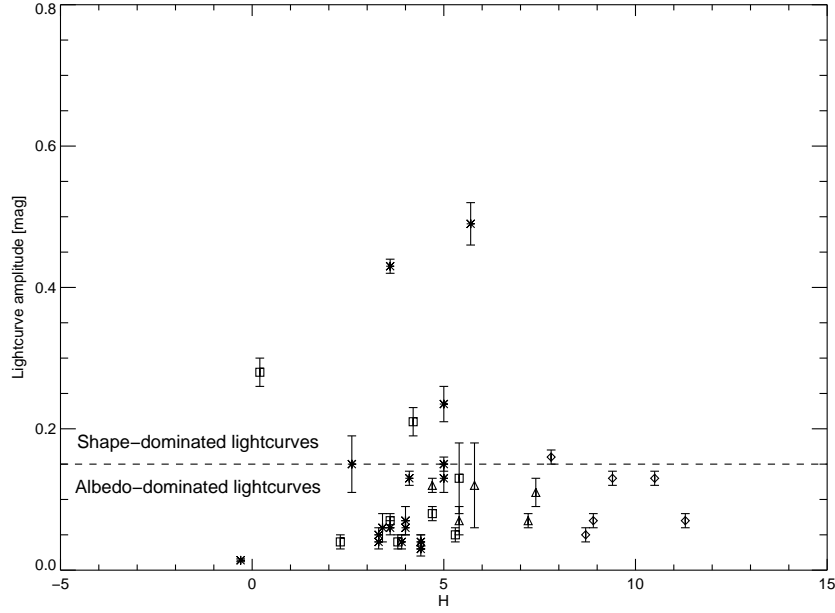


Figure 22. Lightcurve Amplitude vs. Absolute Magnitude: All objects presented in this work and in Thirouin et al. (2010) are plotted: squares for Resonant Objects, asterisks for Classical Objects, triangles for Scattered and Detached disk Objects and diamonds for Centaurs. As mentioned in the discussion section, the sample of studied objects is highly biased toward bright objects and we note the lack of lightcurve with high amplitude. In fact, except, cases like 2001 QY₂₉₇, Varuna or Haumea, majority of studied objects present a low amplitude. Line at 0.15 mag is indicating the separation between the shape and albedo dominated lightcurves. Absolute magnitudes extracted from the MPC database.

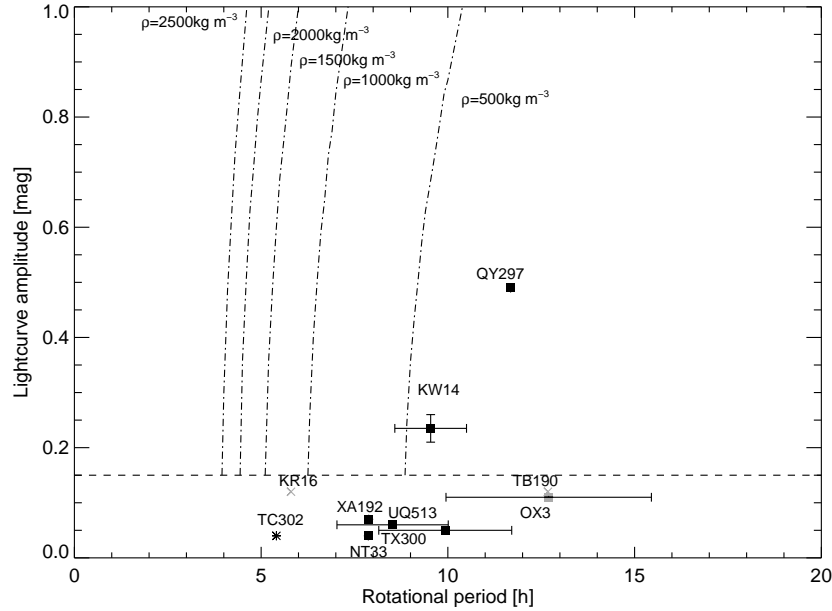


Figure 23. Lightcurve Amplitude vs. Rotational Period for theoretical Jacobi ellipsoids of various densities compared with observations. All objects presented in this work are shown: black crosses for Resonant Objects, black squares for Classical Objects, gray squares for Scattered disk Objects and gray cross for Detached Objects. For each target, we indicate the last part of its name. For example, 2001 QY₂₉₇ is indicated as QY297. In the case of various rotational periods are found for the same target, we plot the average value and the corresponding error bars. Horizontal line defines the separation between shape and albedo dominated lightcurves as in the previous plot. Each vertical dash line defines a density value. Density values are indicated on the top of each line. This plot is updated from Duffard et al. (2009) in which a complete explanation of the plot can be found. This study assumes that TNOs are in hydrostatic equilibrium.

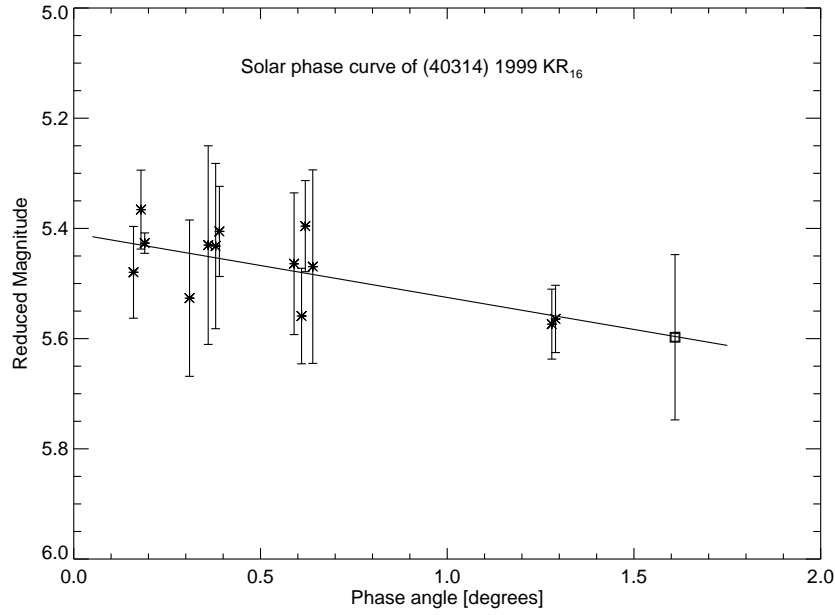


Figure 24. Reduced Magnitude vs. Phase Angle for (40314) 1999 KR₁₆: we plot data published in Sheppard & Jewitt (2002) with an asterisk symbol and data reported in this work with a square symbol. Continuous line is a linear fit of all data.

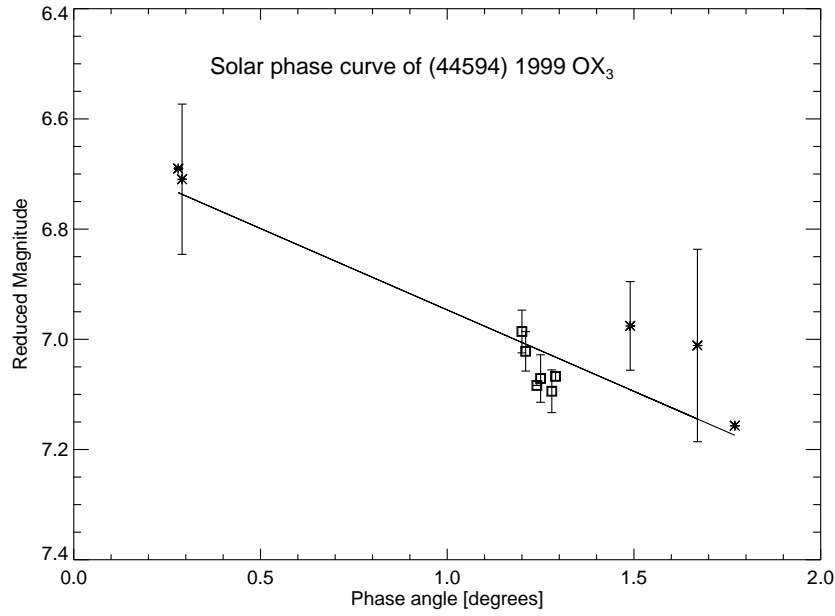


Table 3: This full table is available online. We present our photometric results: the name of the object and for each image we specify the Julian date (not corrected for light time), the Relative magnitude [mag] and the $1\text{-}\sigma$ error associated [mag], the R magnitude [mag], the filter used during observational runs, the phase angle (α) [deg], topocentric (r_h) and heliocentric (Δ) distances [AU] and the magnitude [mag] at 1 AU from the Earth and at 1 AU from the Sun. We highlight in bold face the date of the image in which we performed a crude absolute calibration (see Data Reduction section).

Object	Julian date	Relative magnitude	Error	R magnitude	Filter	α	r_h	Δ	$m_R(1,1)$
(40314) 1999 KR ₁₆	2455039.46074	0.028	0.019	21.19	R	1.61	35.913	36.034	5.63
	2455039.46466	0.100	0.018	21.24	R	1.61	35.913	36.034	5.68
	2455039.46887	0.044	0.018	21.31	R	1.61	35.913	36.034	5.75
	2455039.47279	0.032	0.016	21.31	R	1.61	35.913	36.034	5.75
	2455039.49869	0.050	0.027	21.20	R	1.61	35.913	36.034	5.64
	2455039.50493	0.070	0.031	21.21	R	1.61	35.913	36.034	5.65